Cepstral Analysis of Wideband Ultrasound

By

Eyob Adugnaw

In Partial Fulfillment of The Requirements for The Degree of Master Science

In Biomedical Engineering

(Bioinstrumentation and Biomedical Imaging)

Center of Biomedical Engineering

Addis Ababa Institute of Technology

Addis Ababa University

Advisor

Advisor: Dawit Assefa Haile (Ph.D.)

March 2021

Addis Ababa, Ethiopia

Declaration

I, the undersigned, declare that this thesis is my original work. It has never been presented or published for a degree in any other institution. All sources of materials used in this thesis are acknowledged properly.

Signature: _____

Date: _____

This MSc. thesis has been submitted for examination with my approval as an advisor.

_____

Dawit Assefa Haile (Ph.D.)

Certificate of examination

Addis Ababa University

School of Graduate Studies

This is to certify that the thesis prepared by Eyob Adugnaw entitled *"Cepstral Analysis of Wideband Ultrasound"* submitted in partial fulfillment of the requirements for the degree of Master of Science in Biomedical Engineering (Bioinstrumentation and Imaging) complies with the regulations of the University and meets the accepted standards with respect to originality and quality.

Signed by the examining committee

Examiner: _____Signature: _____Date: _____

Examiner: _____Signature: _____Date: _____

Advisor: _____Signature: _____Date: _____

_____

Graduate program coordinator

Abstract

Ultrasound is a pressure wave with frequency beyond $20\ kHz$. Wideband ultrasound is ultrasound pulse with mega range of frequency components. Most of the currently available ultrasound transducers are narrow banded and fail to provide better axially resolved images for tissues with multiple layers. The methodology used in this thesis models multi-layered biological medium based on linear acoustics of pulse-echo detection principle, normal incidence, longitudinal ultrasonic propagation and investigates the feasibility to detect periodicity. Ultrasound propagation data was generated synthetically and subjected to cepstral analysis to detect periodicity in a multilayered skin tissue model. Rectangular pulses with a center frequency of 16-30 MHz and pulse duration of $1.2 \times 10{-}7s$ and $0.8 \times 10{-}7s$ were applied to a 4-layered medium. The output is measured and cepstral analysis was applied to determine the feasibility of periodicity detection. For layers separated by equal thicknesses, the cepstral peaks existed at equal intervals where as in the case of different layer thicknesses, peaks existed at integer multiple of the thinnest layer thickness. In cepstral analysis, when the cepstral peaks exist at equal intervals or integer multiples of the shortest time of flight (time of flight to the thinnest layer), periodicity detection is guaranteed. It is concluded that periodicity is detected with wideband ultrasound pulses and the minimum and maximum bandwidth are determined based on the duration of the pulse. The possible limitations with the thesis are the assumption of normal incidence planar waveforms, linear ultrasound propagation, and parallel surfaces.

Key words: Cepstrum, Wideband, Pulse, Ultrasound, Layer, Periodicity

Acknowledgment

First, praise and thanks to God, the Almighty to whom I owe my very existence, for the strengths and His blessings in completing this thesis.

I am greatly thankful to my supervisor Dawit Assefa (Ph.D.), for his unreserved support, professional guidance, and constant encouragement from the beginning of this work to the end.

My second thank goes to Michiel Postema (Prof.) from the School of Electrical and Information Engineering at the University of Witwatersrand, South Africa for his valuable ideas, recommendations, and directions to accomplish the study.

Besides, I would like to express my sincere thanks to Seifu (Ph.D. student at AAiT, SECE), for his useful scientific discussions and friendly conversations.

Finally, I pass my deepest recognition to my parents, for their love, support, and understanding.

Table of contents

Contents **Page**

Table of Figures

List of Tables

List of Abbreviations

A-mode	**A**mplitude mode
B-mode	**B**rightness mode
BW	**B**and**w**idth
CT	**C**omputed **T**omography
CW	**C**ontinuous **W**ave
DB	**D**ecibel
FBW	**F**ractional **B**and**w**idth
FFT	**F**ast **F**ourier **T**ransform
HVT	**H**alf **V**alue **T**hickness
M-mode	**M**otion mode
MRI	**M**agnetic **R**esonance **I**maging
PW	**P**ulsed **W**ave
US	**U**ltrasound

Chapter 1 Introduction

1.1 Background

Sound is a mechanical wave created because of the vibration of particles in a medium and transmits energy through its propagation. Ultrasound (US) is a sound wave with frequency beyond$20\ kHz$, the highest audible frequency. Animals like bats and dolphins use ultrasound to locate objects. Bats can emit sound of frequency around $25\ kHz$, and dolphins around $125\ kHz$[1][2].

Wideband ultrasound refers to ultrasound pulse which consists of wide range of ultrasound (>0.5 MHz)[3]. The calculation of the bandwidth (BW) requires the identification of the peak of the frequency response (center frequency *fc*) and a threshold level at a reduction of 6 dB relative to this peak. The bandwidth is then defined as the absolute difference between two extreme frequencies where this threshold is met [4].

The mode of US propagation can be longitudinal or transversal. A longitudinal mode is where the particles are vibrating along the direction of US propagation and transversal mode implies vibrations of particles perpendicular to US pulse propagation. These modes of propagation are determined by the medium through which the wave is propagating. Ultrasound in soft tissues is considered as a longitudinal wave that the direction of the wave and particle motion is parallel. Transversal waves can be found in solid media, such as bone in the biological medium [2].

The intentional use of US started with the sink of the Titanic in 1913. Medical ultrasound was developed in the 1950s following the application of SONAR (Sound Navigation and Ranging). The term SONAR implies locating an object by knowing the direction and distance of the echoes. The principle of locating was implemented by sending a pulse of the sound wave into the ocean [2]. Upon the application of a sound pulse, parts of the wave are reflected after it interacts with a solid object. The reflected wave is received and detected by the hydrophone (underwater microphone) [2][3].

Companies started developing US system suitable for imaging fetuses and the internal body system in the early 1960s. Three years later, I. McDonald and T.G. Brown developed the first commercially successful diagnostic US imaging system.

Medical ultrasonic imaging can be considered as the other version of SONAR, where the ocean is replaced with the human body with important differences. One difference is that SONAR is in the audible range of frequencies while US is beyond the audible range and the medium is another difference. Ultrasound emitted from a medical transducer is of much higher frequency typically in the range $2-20MHz$ for diagnostic purposes [5][6]. The reason for using a much higher frequency than audible sound is to obtain better lateral resolution images.

Ultrasound is the most frequently used, second only to standard x-rays, aging modality in the world for many diagnostic medical applications. Over 25% of all medical imaging procedures involve US and complements the other major imaging modalities, i.e. x-rays and magnetic resonance imaging [3], [4]. It is non-radiative, safe, portable, painless, and cheap as compared to MRI or CT. In certain applications, such as fetal imaging, it is assumed the only modality considered safe [4]. It is also extensively used to image moving structures to measure blood flow in arteries and veins to identify blockage of blood vessels.

The ultrasonic transducer is the basic component of an ultrasonic system responsible for generating US and recording the echoes generated by the medium in the pulse-echo method [8]. Since the transducer should make mechanical vibrations in the megahertz range, the transducer material should be vibrating fast. Piezoelectric materials are common for this. It either can generate waves in continuous or pulsed mode when used in medical applications. In pulsed ultrasound, it is possible to determine the time delay between transmission of the pulse and the arrival of returning echoes to determine how depth-reflecting surfaces are from the transducer. Contrary to the pulsed US source, continuous US is not suitable for the generation of distance measurements [6], [9].

When considering the propagation of US through a medium to its intended site, concepts such as reflection, transmission, and absorption are taken into account. The attenuation experienced by an ultrasonic pulse is frequency-dependent. Attenuation increases with increasing frequency and will limit penetration depth. The transmission coefficient determines the portion of the US beam that is transmitted and the reflection coefficient indicates the portion of beam that is reflected. These coefficients are determined by the acoustic impedance of the two media [10].

The resolution provided by MRI, x-ray and conventional US is approximately 1 mm [7], ruling them out as suitable techniques. Confocal microscopy demonstrates a high resolution in the order of microns, but with a tradeoff imaging depth of approximately 0.35 mm [8]. High-frequency ultrasound can image full thickness with the required resolution. Shorter pulses or wide bandwidth enhances axial resolution, as is the lateral resolution by higher center frequencies [7]. A frequency of 50 MHz has penetration depths of 5 mm and axial and lateral resolutions in the order of tens of microns [11]. This makes high frequency suitable for the lateral resolution. But axial resolution can be upgraded using a wide bandwidth or narrow pulse width [12]. Mathematically, axial resolution is inversely related to the speed of wave and pulse length and directly related to bandwidth. Lateral resolution is inversely proportional to wavelength and focal depth and directly with transducer aperture [13].

The principle of listening to the sound generating the US wave and detecting an echo of a transmitted US signal after reflection from a target involves non-linear US propagation [14]. However, US image interpretation is subjective and relies on the discretion of practitioners [7]. The necessity for standardized diagnosis is considerable for the reduction of misdiagnoses.

This thesis aims to detect and analyze the periodicity of pulsed wideband US in a multi-layered biological media model. Human skin is considered as a three-layered structure and it is believed that deviations in these layers are indicative of anomalies. Detection of these layers and any associated deviations would be of diagnostic value. The cepstral analysis is chosen as a method in detecting periodicity that is exhibited by deterministic structures and it is believed that this periodicity can be used to infer information regarding the layeredness of the skin [7]. The cepstrum is the inverse Fourier transform of a log spectrum, and thus concentrates periodic spectrum components, such as families of equally spaced harmonics and sidebands into a small number of components called rahmonics in the cepstrum [1].

1.2 Statement of the Problem

Most of the currently available US transducers are narrow banded and of course, good in terms of sensitivity and lateral resolution, relatively simple to fabricate, but fail to provide highly axially resolved images for tissue with multiple layers. Moreover, adequate researches are not undergone in determining the possibility of detecting periodicity for the wideband US

in multilayered biological tissues. The existing research works are not considering the effect of attenuation and acoustic impedances of small layers in the tissue. Therefore, research has to be done in this area to decide the possibility of detecting periodicity in the layered biological media. Periodic detection of ultrasonic echo is the key factor to determine reliability of the ultrasonic image. Because if the periodicity of ultrasonic echo is not detected and go for using such transducers will produce normal tissues as abnormal or vice versa.

1.3 Objective

1.3.1 General Objective

Detecting the periodicity of wide-band ultrasound pulse signals in multi-layered biological media.

1.3.2 Specific Objectives

- To generate a pulsed ultrasound signal.
- To determine the bandwidth that propagates through repetitive human tissues
- To determine the possibility of determining periodicity in a multilayered medium.
- To investigate the variation of layer thickness in periodic detection.

1.4 Literature Review

The interest in analyzing signals with the cepstrum approach started in 1963 by B.P. Bogart. He defined cepstrum as “the power spectrum of the logarithm of the power spectrum.” Initially, cepstrum was developed to find echoes in seismic signals from earthquakes or explosions so that the depth of the seismic is determined from the echo delay [1].The approach further started to be used for determining the voice pitch of speech [14]and so speech analysis was one of the earliest applications.

In 1996, M. Postema used the concept of cepstrum to discriminate quarry blasts and microearthquakes. In this study, the medium function was characterized by the Dirac delta function and convolved with the source function (signals generated from the earthquake with different frequency components). Cepstrum analysis was also used for discrimination of ripple firing events from shallow earthquakes [15] and the identification of gearbox faults [16]. When the pattern of the detected waveform deviates from the expected (standard), the gearbox is determined to be faulty. According to [16], cepstrum analysis can detect another form of periodicity characterized by the presence of sidebands spaced at equal intervals around one or several carrier frequencies. In 2018 [10], another author used the concept of

cepstrum analysis in wideband US to detect periodicity. However, the work considered layers at equidistance, same reflection and transmission coefficient, and the same attenuation coefficient to all layers.

The evaluation of small skin tumors performed based on 20 MHz ultrasonic systems using A-scan US imaging was performed in a previous study [17]. The study showed that comparison of echo amplitude, regularity and density yield the most substantial differences between tumors and normal skin. Assessment of skin tumors using B-scan US performed in another study [18] showed a good correlation between histology and US for measurement of tumor depth. The study visualized normal skin and evaluated 200 subcutaneous skin lesions using a 20 MHz ultrasound. The study deduced that high-frequency diagnostics are restricted to the non-intrusive measurement of skin depth and they cannot be used for discrimination between malignant and benign skin lesions. Both works reported in [17] and [18] focused on the $20\mathrm{MHz}$US system. Oppenheim and Schafer [19] published a research paper on "the early history of the development of the cepstrum" but their paper primarily covered applications in speech analysis, communications, seismology and geophysics, and no medical applications including biomedical engineering were considered. The methodology reported in [19] provided a basis for the methodology that is now commonly used regarding cepstrum analysis and numerical simulation of US layer propagation. A bone was modeled as three parallel layers subjected to a short ultrasonic pulse and the reflections were analyzed using the Cepstrum method. Another study reported in [20] assessed the morphological changes in chronic liver diseases using US with the aid of cepstral analysis. In the study, spaces between semi-regularly arranged scatterers representing the liver tissue were measured using cepstral analysis.

The prior solutions presented above show that little to no research has been conducted in the detection of anomalies within the human skin using cepstrum analysis on a wideband US pulse. Moreover, research is not widely done on the repetitiveness of the wideband US in a multilayered medium to maximize the axial resolution.

1.5 Significance of the Thesis

Ultrasound resolution is the most important parameter in medical diagnostics. The findings of this thesis study could tell us the possibility of periodicity detection in wideband US propagating through multilayered biological media and that can lead to a better axial resolution during US imaging. The thesis result also will open a way to resolve thin tissue layers using wideband US. Furthermore, the study might stimulate manufacturers to bring to the market US transducers with a short spike of pulse (wide banded transducers).

1.6 Scope and Limitations of the Thesis

This thesis focuses on the feasibility of detecting periodicity in wideband US waves assuming a multilayered medium. The following assumptions and limitations were considered:

- The US pulse was generated synthetically.
- Thin and parallel tissue layers are assumed.
- Linear acoustics and longitudinal waves were assumed.
- The analysis of nonlinear US propagation and consideration of reverberant echoes are beyond the scope of the current thesis work.
- The minimum and maximum bandwidth over which periodicity can be detected is another limitation.

1.7 Organization of the Thesis

The rest of the thesis has been organized into five chapters. In Chapter 2, the basic concepts and physics of medical US imaging and relevant concepts on ultrasonic resolutions are discussed. Chapter 3 illustrates the approaches of detecting an echo and periodicity with detailed mathematical functions. Chapter 4 explains the methodologies and procedures proposed in this thesis for the effective detection of periodicities in a layered medium. While Chapter 5 presents selected results with useful discussions. Chapter 6 gives a summary and discussion of the research findings in this thesis, their implications as well as recommendations for possible future research.

Chapter 2. Ultrasound Imaging

The interaction of US waves with different tissue types can generate an image. Sound represents mechanical energy that travels through a medium as a longitudinal wave with an alternating sequence of compression and rarefaction of its constituent particles. Rarefaction is a decrease in the density of the medium or the opposite effect of compression [21]. The compression of the medium is represented by positive displacement of the wave's pressure amplitude, while rarefaction closely follows the compressive event with a mirrored response of negative displacement of the wave's pressure amplitude.

2.1Propagation of Sound

Historically, the basis of US imaging traced back to the time of Lazzaro Spallanzani, an Italian physiologist and biologist. In 1790, he discovered that bats navigate (see Fig. 2.1) in the dark using their hearing rather than sight through the reflection of high-frequency sounds (echolocation)[6], [22],[23]. Following this discovery, several scientists and physicists were inspired to study the nature of sound and production of US image for diagnostic and therapeutic purposes.

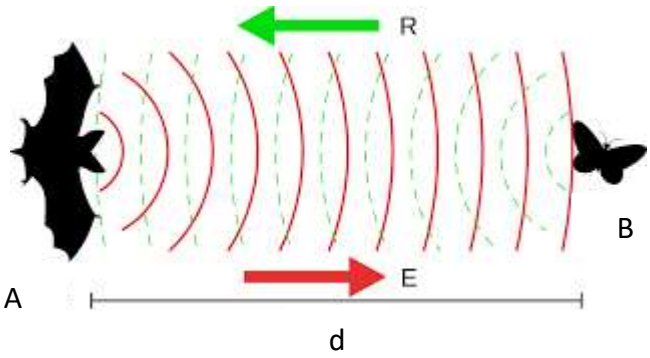

https://www.pngegg.com/en/png-ejhfd

Figure 2.1 Echolocation by animals.

The potential of the US as a diagnostic imaging modality was realized after the end of World War II, derived from underwater SONAR research [23]. In the early 1950s, John Wild and John Reid in Minnesota developed a prototype brightness mode (B-mode) ultrasonic imaging instrument [24], [6], [22]. In 1955, the earliest ultrasonic Doppler devices for monitoring tissue motion and blood was developed by two Japanese investigators, Shigeo Satomura and Yasuhara Nimura.

Ultrasound rapidly progressed through the 1960s from simple “A-mode” scans to “B-mode” applications and compound “B-scan” images using analog electronics. Advances in equipment design, data acquisition techniques and data processing capabilities have led to electronic transducer arrays, digital electronics, and real-time image display [23]. The scope of US and its applications in diagnostic radiology and other areas of medicine progressively changed.

Today, US is the second most utilized diagnostic imaging modality in medicine, second to conventional x-ray, and is a critically important diagnostic tool of any medical facility [24], [25]. Now researchers are giving their attention in enhancing the ultrasound imaging system, processing the signal and modifying the hardware materials to bring up with a result that could fill the need of the end-user.

2.1.1 Wavelength, Frequency and Speed

The most determining parameters of US waves are wavelength, speed of sound and frequency. A simple ultrasonic wave has been depicted in Fig. 2.2 below. The *wavelength* (λ) of the ultrasound energy is the distance between compressions or rarefactions and the *frequency* (*f*) is the number of times the wave propagates through one cycle each second(*s*)[26].

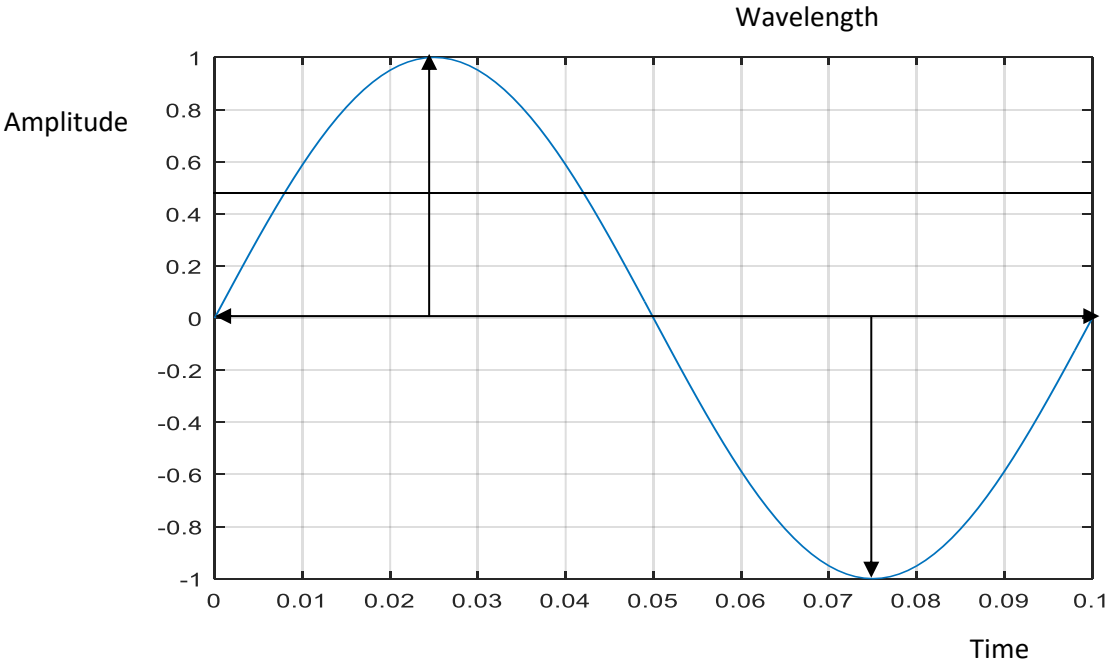

Figure 2.2 Ultrasonic pressure wave.

Sound waves with frequencies less than 20 cycles per second (Hz) are called infrasound, and the range between 20 Hz and 20 kHz comprises the audible acoustic spectrum. Ultrasound

represents the frequency range above 20 kHz. Medical US uses frequencies in the range of 2 to 20 MHz [5], with specialized US applications up to 50MHz. The *speed of sound (C)* is the distance traveled by the wave per unit time and is equal to the wavelength divided by the period (inverse of frequency). The speed, wavelength, and frequency for sound waves parameters are related by:

$$C = \lambda f \qquad (2.1)$$

where $C(m/s)$ is the speed of sound in the medium, $\lambda(m)$ is the wavelength, and f $(cycles/s)$ is the frequency. The speed of sound is dependent on the propagation medium and varies widely in different media [25], [26]. The wave speed is determined by the ratio of the bulk modulus (*B*) (a measure of the stiffness of a medium and its resistance to being compressed) and the density (ρ) of the medium:

$$C = \sqrt{\frac{B}{\rho}} \qquad (2.2)$$

SI units are $kg/\ (ms^2)$, kg/m^3 and m/s for B, ρ and C, respectively. The axial resolution of the US image and the attenuation of the US beam energy depend on the wavelength and frequency, respectively. Ultrasound wavelength affects the spatial resolution achievable along the direction of the beam. Ultrasound wave with high frequency has a shorter wavelength and attenuated easily. Therefore, higher frequencies are not as penetrating but offer better lateral resolution [27]. This explains why high frequencies are used for the superficial body structures and low frequencies are used for those that are deeper. Therefore, in superficial diagnosis, the ultrasonic frequencies can go beyond $20\ Mhz$. Figure 2.3 highlights the different frequency components used in different applications.

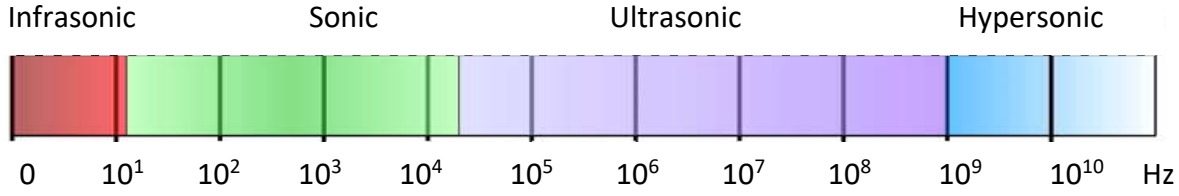

http://www.sengpielaudio.com/calculator-wavelength.htm

Figure 2.3 Sound spectrum.

2.2 Principles of Ultrasound Imaging

Ultrasound imaging is an imaging technique that uses a frequency above the highest human audible frequency range. The typical frequency range used for diagnostic ultrasound is 2 —

$20\ MHz$ [5]. In pulsed wave US imaging, a short spike pulse of mechanical energy is generated and emitted into the tissues and the pulse travels at the speed of sound, despite its dependence on medium, and with changes in the tissue acoustic properties, a part of the pulse reflected as an echo and returns to the source and detected finally. Collection of the echo(s) over time and recording of the echo amplitudes provide information about the tissues along the path of travel. Repeating the process many times with a small incremental change in the direction of the pulse interrogates a volume, from which a gray-scale topographic image (see Fig. 2.2) can be synthesized [23], [26], [28].

www.medison.ru/uzi/eho408.htm

Figure 2.4 Grayscale ultrasound images.

2.3 The skin

Skin is the largest organ of the human body that provides a barrier against the hostile external environment. The skin also prevents excessive water loss from the aqueous interior, the ingress of foreign chemicals and microorganisms and provides strength and stiffness to resist mechanical loading. Other functions of the skin include insulation, temperature regulation and sensation [29], [30].

The human skin is composed of three main layers from the surface to the interior, each with a unique structure and function. These layers are the epidermis, dermis and hypodermis. Mechanical properties (including ultrasonic interactions) of the skin vary considerably and

depend on body site, age, race and gender. The effect of external factors like UV exposure, using creams and individual health and nutritional status can also affect the mechanical properties of the skin [30], [31]. The epidermis and dermis are physically separated by a basement membrane. By contrast, dermis and hypodermis are not physically separated. The basement membrane consists of extracellular matrix components that the epidermis attaches to. This kind of attachment mechanically supports the epidermis.

Thick Skin and Thin Skin

The human skin can be further categorized as thick skin and thin skin. Thick skin is found in the palms and soles. Thin skin covers a large proportion of the body with hairs and is known as hairy skin. Thick skin has more sweat glands and sensory receptors than thin skin. As their names imply, thick skin is thicker than thin skin (see also Fig. 2.5). The thickness of thin skin is around 1–2 mm, whereas thick skin can reach a thickness of 6 mm. This is prominent at the epidermis level where the thick skin epidermis is considerably thicker than the thin skin epidermis [29], [30].

The thickness of the human epidermis ranges from 0.05 to 1 mm, whereas the dermis is about 1–2 mm thick. The thinnest skin is found on the eyelids and the thickest is on the palms and under the soles. The epidermis of eyelids is 0.04 mm while the dermis of eyelids is 0.3 mm. In contrast, the epidermis of the palms and soles is 1.6 mm, whereas the dermis reaches 3 mm [29], [32], [33].

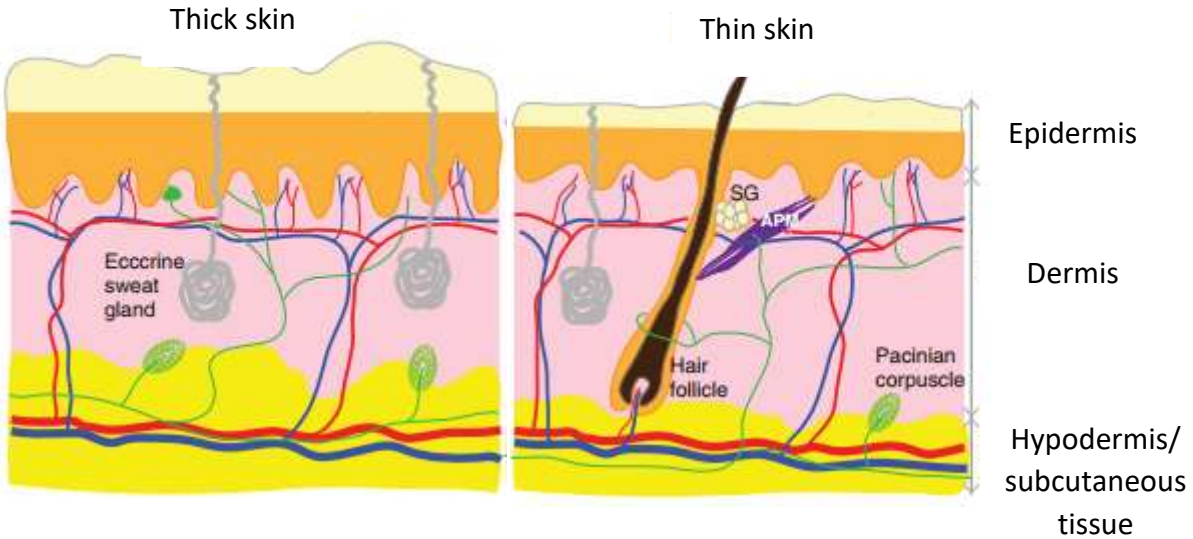

https://opentextbc.ca/anatomyand physiology/chapter/5-1-layers-of-the-skın/

Figure 2.5 (a) thick skin and (b) thin skin.

2.3.1 Epidermis

The human epidermis is a stratified squamous epithelium and is categorized as thin and thick. The epidermis in thin skins consists of four layers of epithelial cells, while in thick skins there are five layers of epithelial cells. In thin skin, from the bottom to the top, or from deep to superficial, the four epidermal layers are:

- The stratum basale (basal cell layer),
- Stratum spinosum (spinous layer or suprabasal layer),
- Stratum granulosum (granular cell layer), and
- Stratum corneum (cornified layer).

In thick skin, an additional layer, the stratum lucidum, is present between strata granulosum and corneum [29]. The five epithelial layers in the epidermis of thick skin have been depicted in Fig. 2.6.

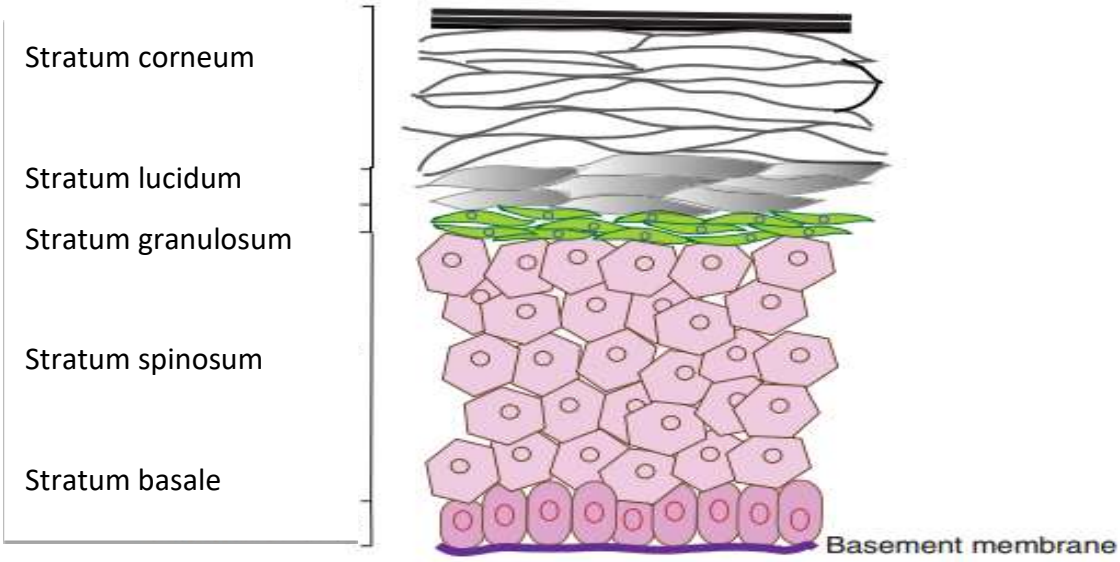

https://opentextbc.ca/anatomyand physiology/chapter/5-1-layers-of-the-skin/

Figure 2.6 Schematic diagram of the five epithelial layers in the epidermis of thick skin.
The stratum lucidum is absent in thin skin. The epidermis is connected to the dermis via the basement membrane.

2.3.1.1 Stratum Basale

The stratum basale is made up of a single layer of basal epidermal cells. Two types of non-epithelial cells, melanocytes and Merkel cells immigrate and reside in the stratum basale.

Melanocytes produce melanin that contributes to skin pigmentation. Merkel cells are thought to function as touch receptors [29], [32]. Merkel cells are more abundant at the fingertips.

2.3.1.2 Stratum Spinosum

The stratum spinosum acquires its name from its spiny appearance in stained specimens. It is also known as the suprabasal layer. The spinous keratinocytes produce water-repelling glycolipids. Overall, the spinous layer contributes to skin strength and flexibility. In addition to keratinocytes, Langerhans cells are also found in the stratum spinosum. Langerhans cells are efficient at recognizing and capturing antigens and other foreign substances in the epidermis.

2.3.1.3 Stratum Granulosum

As its name indicates, stratum granulosum appears grainy. With three to five sublayers, their keratinocytes are flatter in cell shape with the thickening cell membrane. Keratinization begins in this layer; the grainy appearance is generated by keratins and keratohyalin (lamellar granules) in the keratinocytes.

2.3.1.4 Stratum Lucidum

This layer is only present in the epidermis of thick skin, mainly at the palms and holes. The lucidum keratinocytes are lipid-rich proteins that are derived from keratohyalin and contribute to the water barrier function.

2.3.1.1 Stratum Corneum

The stratum corneum is the main layer that contributes water barrier function for the skin. Keratinocytes in this layer are terminally differentiated and nonviable, and they are also known as corneocytes. Corneocytes are filled with keratin filaments.

2.3.2 Dermis

The dermis provides support and nutrients for the epidermis. The dermis is essentially a connective tissue with cells comprising only 10% of its content, while acellular components comprise the majority of its content. The major cell type in the dermis is the fibroblast, spindle-shaped cells that are mainly originated from the mesoderm [29]. Within the dermis, two “layers” of the dermis can be readily observed: the upper layer is the papillary dermis

and the lower layer the reticular dermis, without distinct boundaries. The extracellular matrix meshwork that each layer produces are interconnected. The papillary layer is a loose connective tissue with relatively more fibroblast cells and their collagen fibrils and elastin fibers are thinner and loosely organized. By contrast, the reticular layer is a dense connective tissue. Relatively fewer fibroblast cells are present in the reticular dermis, along with less ground substance [29], [32].

2.3.3 Hypodermis

The hypodermis is primarily adipose (fatty) tissue and the origin of some blood vessels that extend to the dermis. Similar to blood vessels in the dermis, blood supply in the hypodermis acts to supply the skin with nutrients while also acts as the entry to the systemic circulation. Overall, the hypodermis is a loose connective tissue that provides cushioning and blood supply for the dermis and epidermis [29], [33].

2.4 Interaction of Ultrasound with Tissue

To use US for either diagnostic or therapeutic purposes, a beam of ultrasound is directed into the tissues of the subject over a selected area of interest. The ultrasonic wave interacts with the tissues along its line of propagation. In this part, the characteristics of interaction between US and tissue are highly dependent on the biological and chemical makeup of the interacting medium through which the beam passes and the ultrasonic wave parameters (frequency, speed and wavelength) [34].

2.4.1 Acoustic Impedance and Boundaries

Ultrasound images are generated through the interaction of ultrasound waves with tissues of differing acoustic properties. This interaction is highly governed by the acoustic impedance, Z, of the tissue. Acoustic impedance is defined as the resistance of the ultrasonic wave from the transmission and can be calculated by multiplying the density of the medium,$\rho(kg/m^3)$, and the speed of the ultrasound, $C(m/s)$, [22], [35], [36].

$$Z = density\ x\ velocity = \rho C \qquad (2.3)$$

The unit of acoustic impedance is *Rayl* $(kg/m2/sec)$. The acoustic impedance of air is $0.0004\ Rayl$ and that of bone is $7.8\ Rayl$, which are extreme values. The propagation of ultrasonic wave through a medium encounters an interface with an acoustic impedance mismatch. Up on US interaction with the medium, different interactions can occur: reflection,

refraction, absorption, attenuation, or scatter [35]. Figure 2.7 presents an US incident beam hitting an interface between two media and then refracted.

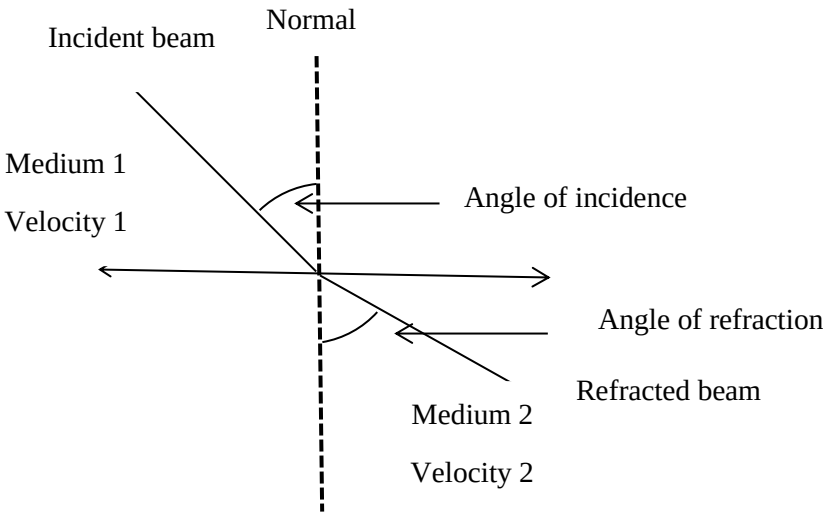

Figure 2.7 Interaction of ultrasound at the boundaries.

In general, the extent to which an acoustic boundary affects a beam of US incident upon it will depend on the magnitude of the difference between the acoustic impedance values of the two structures on either side of the boundary.

2.4.2 Reflection of Ultrasound

Reflection occurs at the interfaces where there is difference in acoustic impedances and is critical to the generation of an US image. The reflected US energy is called an echo. A larger acoustic impedance mismatch results in a larger percentage of the incident energy being reflected [35][37].

The difference in acoustic impedance of the media determines the amount of US reflected at each interface [38]. The amount of sound transmitted and reflected depends on the degree of mismatch between the acoustic impedance of the two media on either side of the interface.

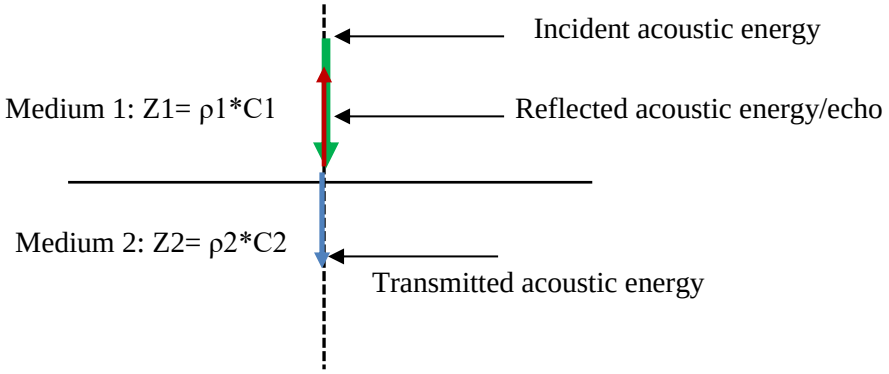

Figure 2.8 Reflection of sound with perpendicular incidence to a boundary layer.

For the perpendicular incidence of the acoustic wave (see Fig. 2.8) at the boundaries of layers with different acoustic impedance, a portion of the beam is reflected and the remaining is transmitted into the next medium [39].The percentage of reflection of ultrasonic waves in a layer boundary is calculated as:

$$RA = \frac{Z2-Z1}{Z2+Z1} x100\% \quad (2.4)$$

Since the percentage of energy reflected and the energy transmitted should give value unity and the percentage of transmission is calculated as:

$$TA = 1 - Ri = (1 - \frac{Z2-Z1}{Z2+Z1}) x100\% \quad (2.5)$$

The ultrasonic wave is almost completely reflected on an interface between air and soft tissue because the acoustic impedance of air is much lower than that of soft tissue.

Besides acoustic impedances, there are also other factors that affect reflection. These are the layer surface characteristics, the size of the layer, and the angle of incidence. When the US propagates through a smooth surface, the incidence angle and the angle of reflection are equal. Increasing the angle of incidence decreases the probability of echo being detected by the receiving transducer. Specifically, if the angle of incidence exceeds 3^0 from the perpendicular layer, the US transducer fails to detect a reflected echo [35], [22]. In this thesis work, the normal incidence of an US pulse is assumed to maximize the probability of the reflected pulse detected.

In addition to the reflection from a single interface between two layers, US will be normally incident and interacting with multiple tissue interfaces. The wave coming from the first layer reaches the second layer and is split into transmitted and reflected waves. After passing through the layer, the transmitted wave is split again at the second interface, and so on, the result is a sequence of reflections in both directions inside the plate[40]. On either side, a sequence of waves leaves the plate which are superimposed and whose total sound pressure has to be determined.

Two types of reflection can occur, depending on the smoothness of the boundary relative to that of the US beam, or high on irregularities of shape on the surface of the reflector. Specular

reflections occur when the boundary is a smooth surface, while non-specular (diffuse) reflections occur when the interface is rough [38] (see Fig. 2.9).

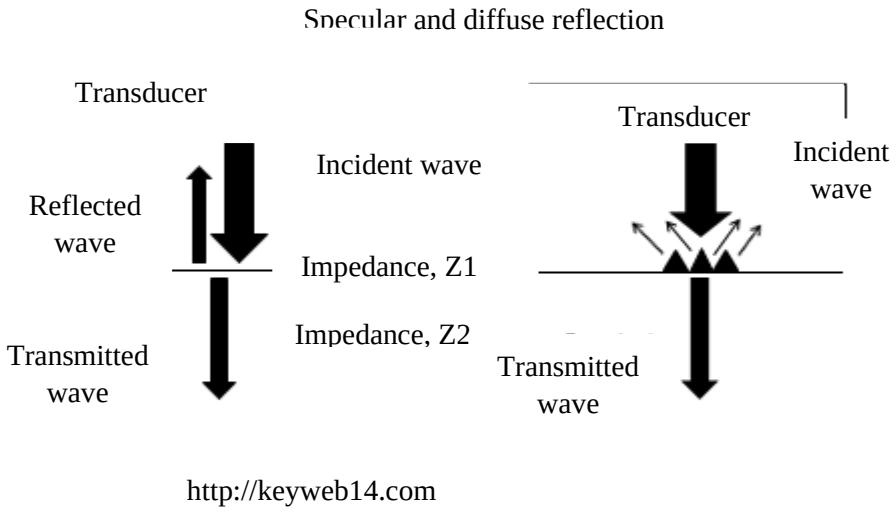

Figure 2.9 Reflections in smooth (left) and rough (right) surfaces.

2.4.2.1 Specular Reflections

It is characterized by the flatness of the interfaces through which the US wave is propagating. The angle of incident pulse and reflected pulse are equal. In the current thesis work, the incident wave is assumed normal to the interface so that the incident and reflected angles are zero. In this normal incidence, the echo goes straight back with a high probability of being picked up by the transducer. Two techniques are commonly used to maximize the probability of the echo detected by the transducer: using a coupling medium (gel)and using impedance matching techniques. The reflected beam is referred to as the echo. The amplitude of an echo due to specular reflection depends on the difference in acoustic impedance values of the two media forming the boundary (acoustic mismatch) [38], [41], [55].

The reflection coefficient (R) can be computed as:

$$R = \frac{Ar}{Ai} = \frac{Zk - zl}{Zk + Zl} \qquad (2.6)$$

where, $Ar =$ Intensity of the reflected echo, $Ai =$ Intensity of the incident beam at the boundary, $Zk =$ Acoustic impedance of the first medium, and $Zl =$ Acoustic impedance of the second medium.

The ratio, called the reflection coefficient, gives us the proportion of beam amplitude reflected from the interface and the echo size in proportion with this coefficient. Its magnitude will be dependent on the acoustic mismatch at the interface [43] (see also Fig. 2.10). For example, the acoustic impedance of soft tissues is quite similar to one another and this produces small echoes. Very large echoes are produced at the air soft tissue interface because there is large difference in acoustic impedance mismatch. The acoustic impedance difference between bone and soft tissue is also large and produce large echoes [55].

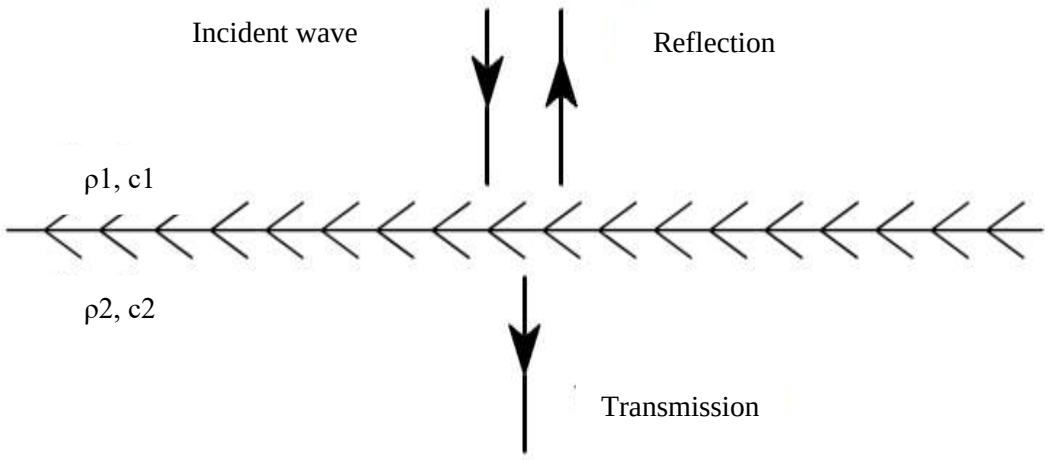

Figure 2.10 Reflection and transmission of ultrasound.

2.4.2.2 Scattering of Ultrasound (Non-Specular/Diffused Reflections)

This refers to the scattering of the beam into different directions due to the irregularities of the reflecting interface. The direction of scattering does not obey the simple law of reflection as in specular reflection. In reality, scattered US provides much useful information about the internal texture of organs. Scattered echoes are much weaker than specularly reflected echoes, but the high sensitivity of modern US equipment makes it possible to utilize information from scattered US for imaging. Scattering shows very strong frequency dependence, increasing rapidly as the frequency of US is increased [42], [55].

2.4.3 Refraction of Ultrasound

Refraction is bending or change of beam direction as also depicted in Fig. 2.11. Ultrasound travels at different velocities in different propagating media. Itis caused by a change of

wavelength as the US crosses from the first medium to the second while the beam frequency remains unchanged [33, 39, 40]. The frequency remains unchanged and the velocity and wavelength vary. Refraction does not contribute to the process of image formation as a reflection does. However, the deviation of ultrasonic energy into new directions contributes to loss of beam amplitude.

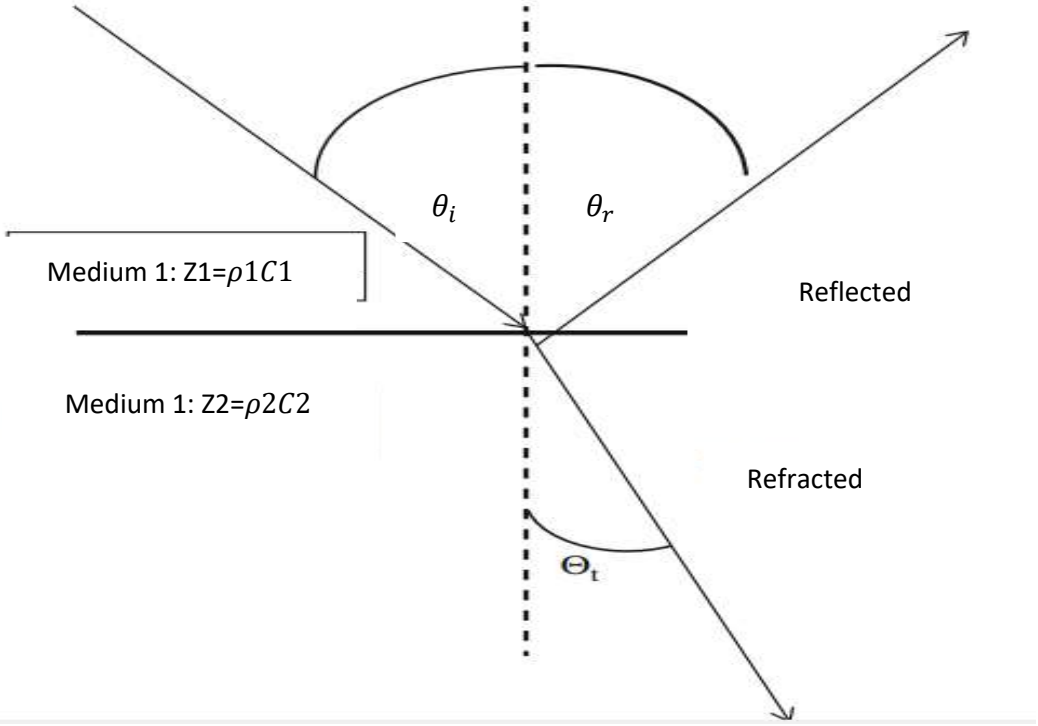

Figure 2.11 Refraction of ultrasound.

2.4.4 Absorption of Ultrasound

Absorption is defined as the loss of US energy as mechanical energy is converted to thermal energy or heat in the propagating medium. With the loss of US energy, there is a failure to transmit sound beyond the interface, leading to the devoid of echoes, the so-called shadowing. The extent of a medium to absorption of US beam is affected by three main variables[55]. These are:

(i) The viscosity of the medium,

(ii) The relaxation time of the medium, and

(iii) The beam frequency.

Viscosity is the frictional force between fluid particles of the medium. Viscose particles resist the propagation of US wave and produce heat. Therefore, absorption of US increases with increasing viscosity

Relaxation time is the time taken by particles to revert to their original mean positions following displacement by an US pulse. When the relaxation time is short, vibrating particles can revert to their original positions before the next pulse, but when it is long, the next pulse may encounter the particles route before they are fully relaxed. Therefore, the longer the relaxation times of a medium, the higher the absorption of US.

The frequency of vibrating particles generates more heat because a high-frequency US beam enforces particles to move with high velocity. For soft tissues, absorption of US increases in direct proportion to the beam frequency. Among materials of biological interest, bone absorbs US much more strongly than soft tissues [46],[55].

2.4.5 Attenuation of Ultrasound in Tissues

Attenuation is the exponential reduction in amplitude or intensity of ultrasound wave during propagation. The term attenuation distinguished from absorption in that absorption relates to the conversion of ultrasonic energy into thermal energy and attenuation refers to the total propagation losses that is dependent on the thickness of the tissue and the frequency of the beam [38], [55].

Mathematically, attenuation is expressed as:

$$I = I_0 e^{-\mu x} \qquad (2.7)$$

where, **I** Is the measured signal, $\mathbf{I_0}$ The source signal, **μ**The attenuation coefficient of the medium and **x** the signal path length.

The attenuation coefficient is related to frequency using the formula:

$$\mu = \mu_o f^n \qquad (2.8)$$

where $\boldsymbol{\mu_0}$ is the attenuation coefficient at a reference frequency, **n** is the power of frequency dependence with attenuation.

Attenuation increases with frequency linearly or nonlinearly based on the biological medium the US signal is propagating through. Bone and lung have power factors of 1.7 and 0.6 respectively and soft tissues relating linearly [41], [47].

2.4.5.1 Ultrasonic Half Value Thickness (HVT)

The attenuation in a specified medium is quantified in terms of distance within that medium which reduces the intensity of the beam to one-half of its original value (HVT). Table 2.1 presents HVT values for different materials for different US frequencies.

Table 2.1 Ultrasonic Half-Value Thicknesses for different materials

Material	**HVT (cm) at different frequencies**				
	1 MHz	**2 MHz**	**5 MHz**	**10 MHz**	**20 MHz**
Blood	17.0	8.5	3.0	2.0	1.0
Brain	3.5	2.0	1.0	-	-
Liver	3.5	1.5	0.5	-	-
Soft tissue (average)	3	2.1	0.86	0.3	0.15
Water	1360	340	54	14	3.4
Bone	0.2	0.1	0.04		
Air	0.25	0.06	0.01	-	-

[McDicken, 1976, pp. 58].

The data in Table 2.1 shows HVT values for different tissues. The HVT for liquids is large and low for bones and gases. This means that US can travel long distances in liquids. The reason for this is that clear liquid is acoustically homogeneous and there are no acoustic boundaries within. On the other hand, bone and gas impede the flow of the US. Bone absorbs heavily while gas boundaries reflect almost totally. Fat impedes the transmission of ultrasonic energy and such materials are referred to as acoustic barriers [48], [49].

2.4.6 Scattering

Scattering is the redirection of US waves as they interact with rough or uneven structures. These tissue interactions occur where there is little difference in acoustic impedance [38], [41].

2.5 Ultrasound Display Modes

After the US echoes are detected and processed electronically, next is to display for viewing and making decisions. Different modes of displaying give us different information [13].

2.5.1 The Amplitude Mode (A-Mode)

In this mode, echo amplitude is displayed on the vertical axis while echo return time is displayed on the horizontal axis. The amplitude of a spike is a relative measure of echo size [50].

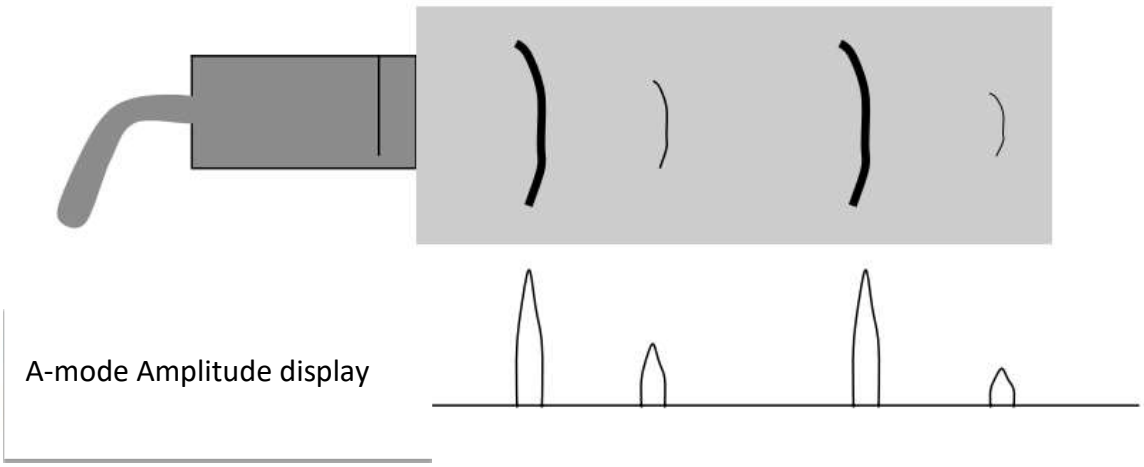

https://www.nysora.com/foundations-of-regional-anesthesia/equipment/physics-of-ultrasound/

Figure 2.12 Display of information in A-Mode.

Each spike corresponds to a reflecting interface along the scan line. The A-mode suffers from the limitation of displaying only 1-D information, representing the echoes lying along the beam path. Hence, the information does not constitute an image.

2.5.2 The Brightness Mode (B-Mode)

In brighten mode dots are represented as the intensity or brightness of echo signals on display. The brightness is a relative measure of echo size. The B-mode display is employed as A-mode in which the vertical axis is replaced with small dots. These dots are existed at tissue boundaries where there is acoustic impedance mismatch. The combined information from different scan lines provides a 2-D image of the cross-section through which the beam sweeps [50], [51].

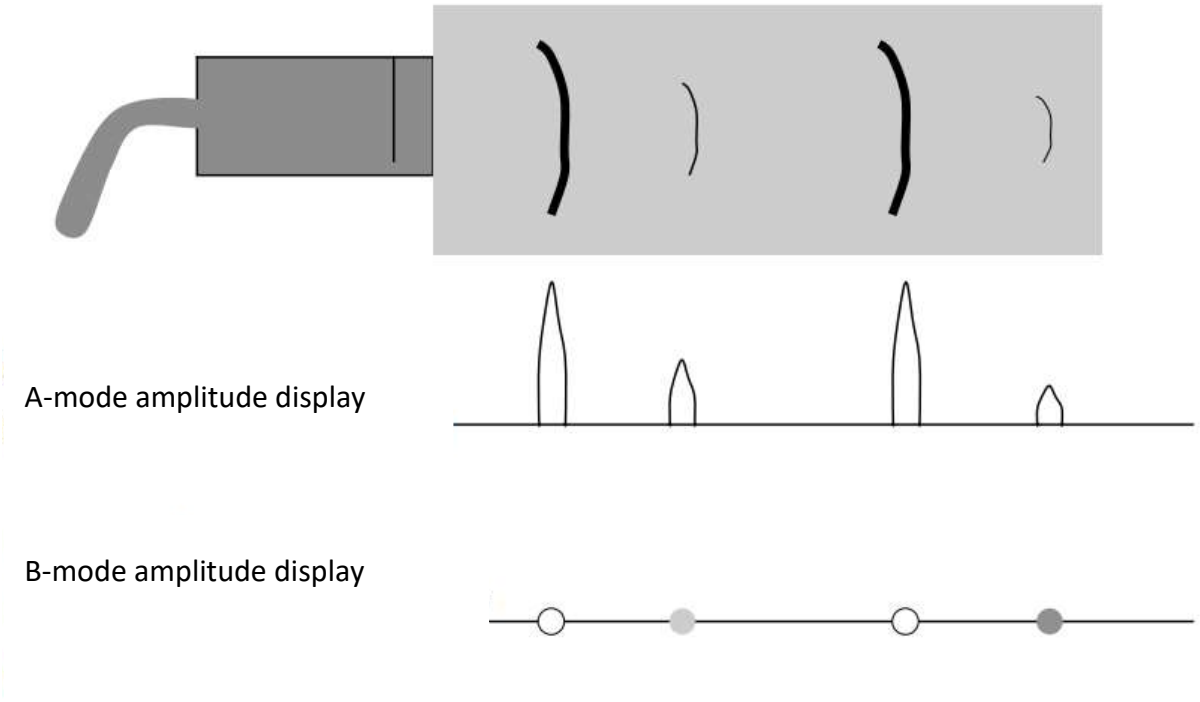

https://www.nysora.com/foundations-of-regional-anesthesia/equipment/physics-of-ultrasound/

Figure 2.13 Display of information in B-Mode.

2.5.3 The Motion Mode (M-Mode)

In M-mode display tissue depth is displayed along one axis and time is on the other axis. The transducer is placed in one fixed position to the moving structure. The M-mode is particularly useful in examining cardiac motion [52].

2.5.4 Real-Time Mode

A succession of images of the same plane is generated and viewed as they are acquired. The effect of rapid acquisition and viewing at rates exceeding about 25 image frames per second creates the impression of continuity in time. This impression arises due to limitations in human perception. Human being is unable to distinguish in time between events occurring at the rate of beyond 25 frames per second. In medical ultrasonics the image is displayed at the rate of 40 frame per second which human being viewing this as appearing at the same time [54], [55].

2.5.5 The Doppler Mode

Doppler is associated with relative motion between the source of the sound and the receiver, resulting in an apparent difference in frequency between that emitted by the source and that

perceived by the receiver. An approaching sound source is perceived to be emitting sound at a higher frequency than it is, while a receding source appears to emit at a lower frequency as also shown in Fig. 2.15 [54], [55].

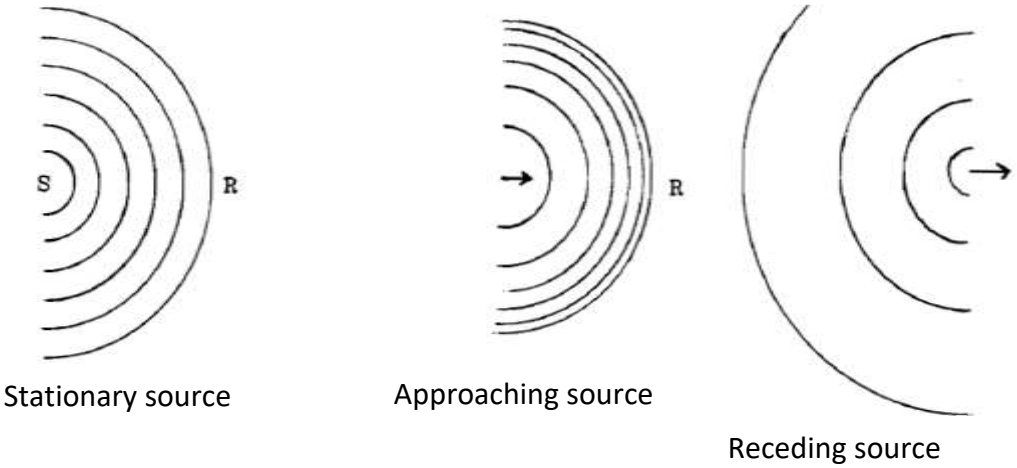

Figure 2.14. Doppler effect.

Wavefronts get compressed for approaching source and decompressed for receding source, as perceived by the receiver.

According to [55], the Doppler shift can be used to:

- Detect motion,
- Determine the direction of motion, and
- Determine the velocity of a moving structure.

Doppler mode is used in studies of blood flow and cardiac movements. An US wave with constant frequency emitted from the transducer interacts with a moving acoustic boundary and the wave gets reflected to the receiver. The shift of frequency is related to the velocity of the moving reflector and the direction of motion. The doppler shift and the velocity of the moving structure are related directly. Higher detected frequency implies relative motion towards the transducer, while a lower detected frequency implies a receding reflector [55]. Figure 2.16 depicts spectral Doppler evaluation of a uterine artery of a subject.

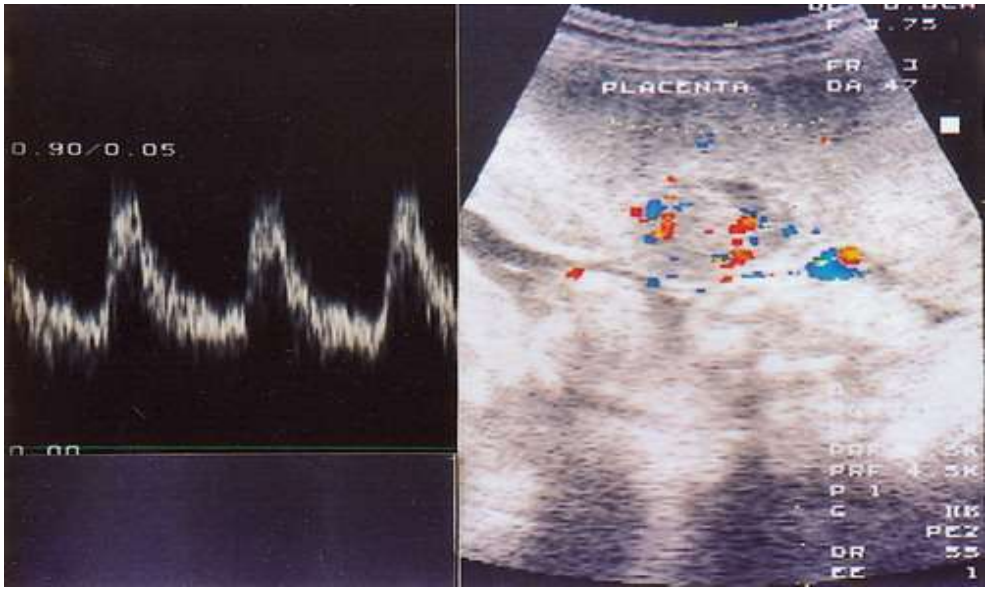

https://pubs.rsna.org/doi/10.1148/radiographics.22.1.g02ja0947

Figure 2.15 Spectral Doppler evaluation of the uterine artery.

2.6 Image Characteristics in Clinical Ultrasound

The quality of a diagnostic image is determining its usefulness. The overall quality of an US image is the collective effect of the imaging system and performance of the operator. The transducer, electronics, signal processing, image processing, display, and recording devices are components of the imaging system that affect the ultimate quality of the US image. Experiences show that unskilled operators generate poor quality images from the very best of equipment [46].

A discussion on the quality of the US image centers on image resolution and contrast. Image contrast distinguishes an object of interest from the surrounding background tissue that contains it. Resolution refers to the ability to distinguish two reflectors visible. For the US image, components of resolution include spatial resolution, temporal resolution, and contrast resolution. It is appropriate to consider the factors, which affect resolution, in some details [55].

2.6.1 Spatial Resolution

Spatial resolution in the US is concerned with the ability to distinguish between two reflectors in space. It has two components. Axial resolution is the ability to distinguish between echoes originating from two reflectors lying one behind the other along the axis of the US beam (see Fig.2.17). It is sometimes referred to as depth or longitudinal resolution. Lateral resolution is

the ability to distinguish between two reflectors situated side by side in a direction perpendicular to that of the US beam(Fig.2.18) [55], [58].

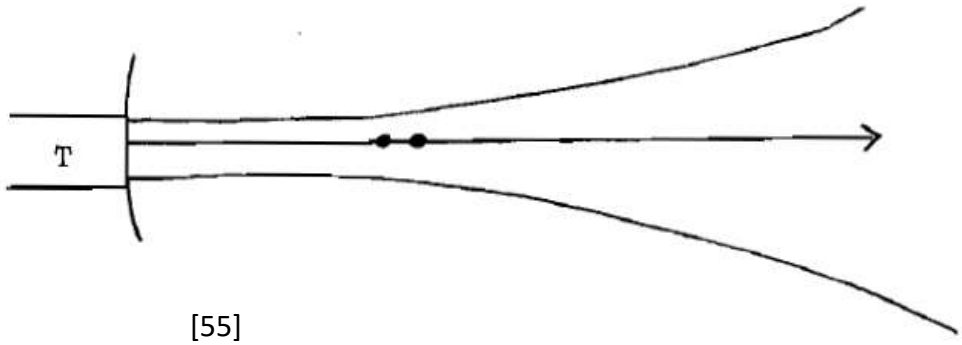

[55]

Figure 2.16 Axial resolution: reflectors lie side by side along the beam direction.

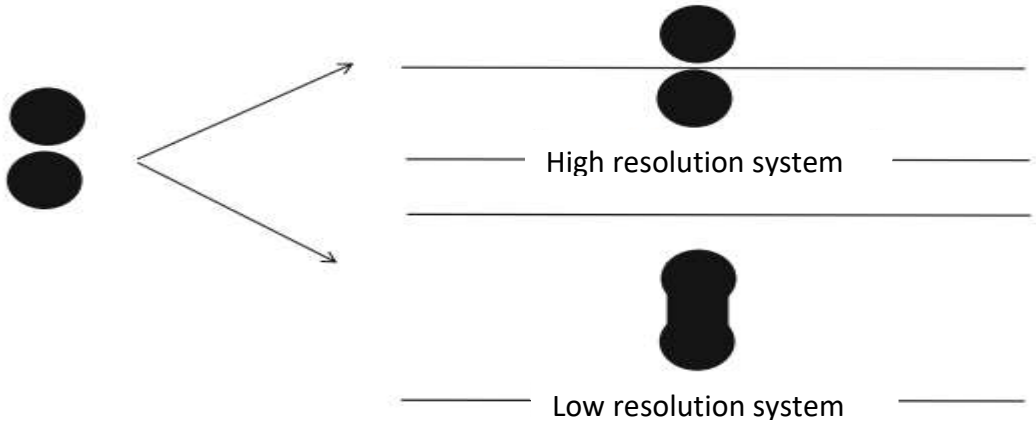

Figure 2.17 Lateral resolution: reflectors lie side by side perpendicular to the beam direction.

2.6.1.1 Axial Resolution

Axial resolution is the minimum distance that can be differentiated between two reflectors located parallel or along the direction of US wave propagation (see Fig. 2.19).

The returning echoes must be distinct without overlap to achieve better axial resolution. The length of the US pulse and the bandwidth highly determine the axial resolution. The pulse length (see also Fig. 2.20) of the US is related inversely proportional to the bandwidth of the pulse. Therefore, a short spike of the pulse will give us a wide bandwidth US signal. In between pulses, there are comparatively much longer (non-generating) intervals during which the transducer serves as a receiver [55], [57].

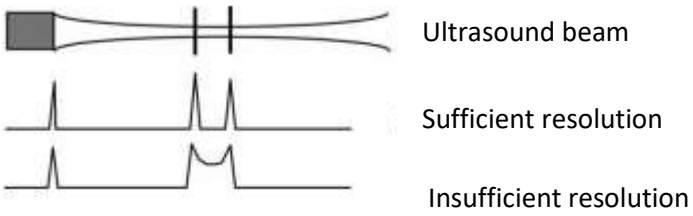

Figure 2.18 Degree of axial resolution: reflectors lie side by side along the beam direction.

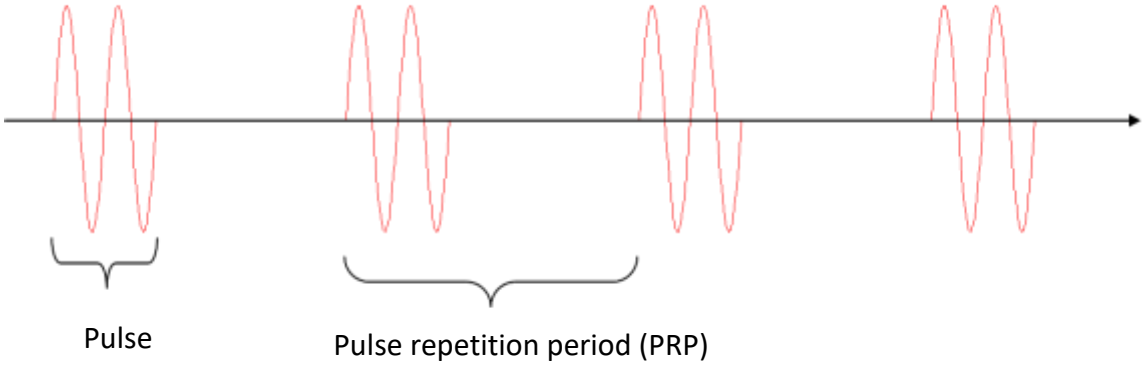

Figure 2.19 Oscillations in pulsed wave ultrasound.

Mathematically, axial resolution can be defined as the half ratio of the speed of US to pulse bandwidth.

$$\boldsymbol{Axialresolution} = \frac{\boldsymbol{C}}{\boldsymbol{2B}} = \frac{\boldsymbol{C\tau}}{\boldsymbol{2}} = \frac{\boldsymbol{SPL}}{\boldsymbol{2}} \qquad (2.9)$$

where τ is the pulse length, C is the speed of sound, SPL is spatial pulse length and B is the pulse bandwidth. The spatial pulse length is the product of wavelength and the number of wave cycles constituting the pulse.

$$\text{Spatial pulse length} = \text{wavelength x number of cycles in a pulse}$$

Small spatial lengths can be achieved with high pulse frequency or short pulse duration (small pulse cycles). But high-frequency US waves are attenuated more and decreasing the pulse duration is the best way to maximize the axial resolution [50]. Objects closer than half of the spatial pulse length are not resolved well.

2.6.1.2 Lateral Resolution

Lateral resolution is the ability to distinguish between two reflectors situated side by side in a direction perpendicular to that of the US beam. The lateral resolution is mainly determined by the size of the probe and the frequency of the beam. It is defined as:

$$L = \frac{\lambda f}{D}, \qquad (2.10)$$

where L is the lateral resolution, D is the transducer aperture, f is the focal depth, and λ is the wavelength. Thus, the resolution improves with larger aperture. It is therefore important that the factors affecting lateral resolution be well-understood [55]. These factors include:

A. Beam width,
B. Beam frequency, and
C. Scan line density.

A. Effect of Beam Width

The lateral resolution is highly limited by the width of the beams whereas axial resolution is by the width of the US pulse. Reflectors are closer to one another than the beam width cannot be resolved (see Fig.2.21). Therefore, the narrower the beamwidth, the better the lateral resolution.

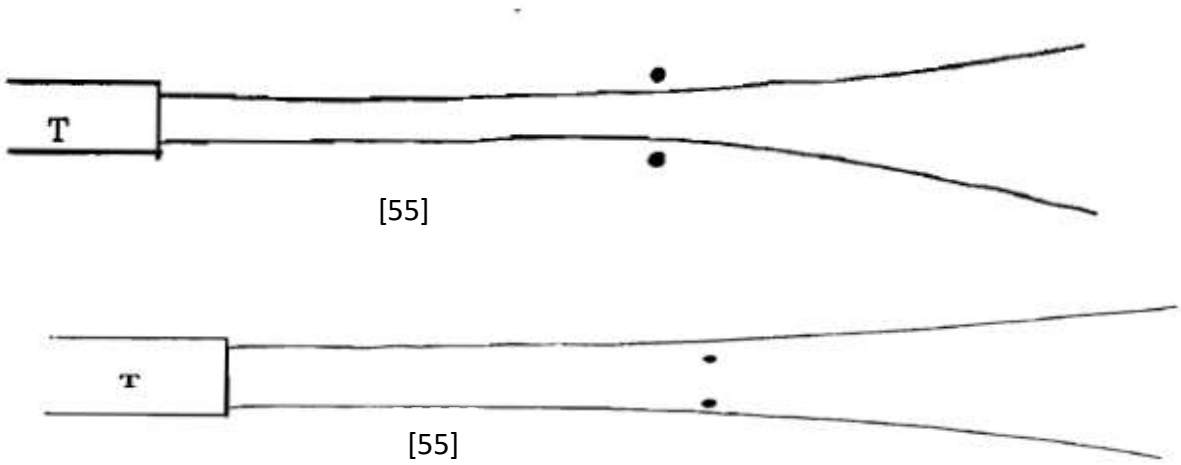

[55]

[55]

Figure 2.20 Effect of beam width on spatial resolution:
Small beam width (top) and larger beam width (bottom).

The lateral resolution is highly dependent on tissue depth, since the beam width may vary widely with distance along the beam path. A simple illustration of axial and lateral resolution has been depicted in Fig. 2.22.

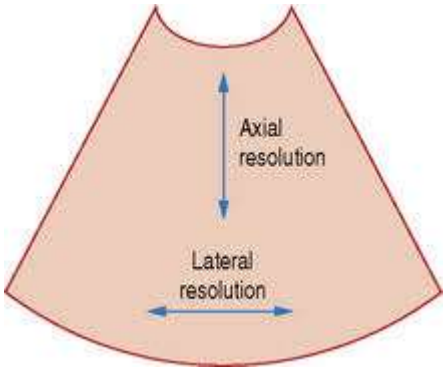

https://www.radiologykey.com

Figure 2.21 Simple illustration of axial and lateral resolution.

B. Effect of Beam Frequency

The frequency of US beam affects the beam shape and the lateral resolution. Beam shape at lower frequencies gets wider and narrower at higher frequencies. Therefore, the higher the frequency, the better the lateral resolution.

C. Effect of Scan Line Density

The combination of echo information from scan lines across the selected area of interest forms an image. The number of scan lines contributing to the image affects the lateral resolution. Sampling the tissues at closer intervals improves resolution. Therefore, the higher the scan line density the better the lateral resolution. The scan line density decreases with distance from the transducer, and hence the lateral resolution is also affected with increasing tissue depth.

2.6.2 Contrast Resolution

Contrast resolution is the ability to resolve between signal sizes. In the context of US imaging, this mean distinguishing between the intensities of the dots representing echoes of US signal of different sizes. Contrast resolution is largely affected by the contrast properties of the display, imaging system and recording devices. The contrast resolution can be improved by appropriate image processing techniques [46].

2.6.3 Temporal Resolution

Temporal resolution is the ability to separate events in time and is important in real-time imaging. The rate at which image frames are generated and viewed affects the visualization of moving structures. The human eye can visualize events with frame rates greater than 40 milliseconds and below this recognized as an event taking place simultaneously. This level of

temporal resolution dictates that the framing rate required for real-time imaging to observe moving structures should be 25 frames per second (f.p.s) or more (if one image frame is generated every 40 milliseconds, then in a total time of 1 second, or 1000 milliseconds, 25 image frames will be generated). Framing rates below about 20 f.p.s are associated with a phenomenon called image flicker, which arises from the ability of the eye to distinguish the resulting image frames as being separate in time [46], [51].

2.7 Sensitivity of the Imaging System

In ultrasonic imaging, sensitivity determines the ability of the imaging system to detect small echoes. The smaller the minimum detectable signal for given energy input, the higher is the sensitivity. Since weak echoes may carry a large proportion of diagnostic information, system sensitivity is a critical aspect of ultrasonic imaging. The transducer and the electronics will determine the size of the ultrasonic pulse transmitted into the body. The transducer converts electrical energy into mechanical energy at transmission and mechanical energy into electrical energy at the reception of echoes in the case of reflection mode US. The responses of the display and recording systems to incoming signals depend on the inherent sensitivity characteristics of the display and the recording media.

Chapter 3. Echo and Periodicity Detection

3.1 Echo Detection

Ultrasound signal that has propagated through a layered medium is the convolution of the source function and a function representing the layering of the medium in the time domain [61]. The source function represented as a rectangular modulated sinusoid pulse with a specific propagating frequency and pulse width. The pulse width has to be less than or equal to the minimum time of flight (the minimum ratio of thickness to velocity). The media function a type of Dirac's delta function $\sigma(t - ndt)$, which response at the interface of the layering tissue where these interfaces are present [10], [12]. Dirac's delta function is used to effectively model short living ultrasonic echo responses at the boundary between layers. The echo is produced from the convolution of the source function and the medium function provides diagnostic information about the tissues. The minimum thickness determines the minimum pulse duration assuming that the pulse propagates with the same speed throughout the tissue. After the echoes are detected at different interfaces, it is important to decide whether the detected signals are periodic or not. Non periodic signal implies anomalies (abnormalities) within the tissue the US signal is passing through. Two techniques can be used to detect the periodicity of an echo. The first technique involves an analytic approach using simple algebraic mathematical functions. The other method is Cepstral analysis that can help us determine the extent of periodicity.

Considering $h(t)$ as impulse response of the media function and $x(t)$ as source function, the convolution of these two functions will give us the detected echoed signal $y(t)$ as also depicted in Fig. 3.1.

$$y(t) = x(t) * h(t) \qquad (3.1)$$

3.2 Cepstrum Method

Cepstrum is a useful signal processing technique and involves taking the inverse discrete Fourier transform of the log magnitude spectrum. The cepstrum analysis has many applications in geophysics, pitch determination, mechanical material analysis and biological applications [62].

The first article published in 1963 [63] defined Cepstrum analysis as ''the power spectrum of the logarithm of the power (Amplitude) spectrum'' of a signal. The approach was designed to

the detection of echoes in seismic signals over autocorrelation function. The paper defined Cepstrum as function of pseudo time, τ, pseudo magnitude, gamnitude and the spectral ripple frequency or Quefrency. The author further redefined the following terms

Spectrum	*Cepstrum*
Phase	*Saphe*
Amplitude	*Gamnitude*
Filtering	*Liftering*
Harmonic	*Rahmonic*
Period	*Repiod*

Cepstrum was used to find echoes in seismic signals from earthquakes or explosions to determine the depth of the seismic signal from the echo delay [64]. It has also been used for the identification of gearbox faults [16], discrimination of ripple firing events from shallow earthquakes [12], determination of the thickness of a layer made of a variety of materials, (for example, ceramics, semiconductors and soft tissues) [65], [66], and determination of the R peaks and the distance between these peaks. According to the study in [63], Cepstrum analysis can detect another form of periodicity characterized by the presence of sidebands spaced at equal intervals around one or a number of carrier frequencies and known as scalloping.

In all application areas, Cepstrum is used for detecting the periodicity and calculating the thickness of the target layer (s) in the frequency spectrum [16]. Two commonly used techniques used in Cepstral analysis are power (amplitude) Cepstrum and complex Cepstrum [62]. Complex and imaginary Cepstral analysis techniques retain the phase information and used if we are interested in recovering the processed signal into its original signal. Amplitude or power spectrum-based analysis fails to recover the original signal since the phase information will be lost. Amplitude or power Cepstrum is used if one aims to detect the periodicity or measure the thickness of the layer despite recovering the original signal. In the current thesis work, the amplitude Cepstrum is used to detect the periodicity of wideband US signal as the phase information is not required to obtain the original signal as the signal is already generated synthetically. A rough block diagram of the Cepstral analysis procedure has been depicted in Fig. 3.2.

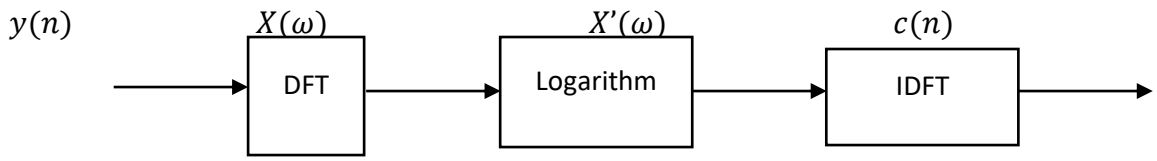

Figure 3.2 Block diagram of cepstrum

$$y(t) = x(t) * h(t) \quad (3.2)$$

The above convolution equation in the time domain translates to a multiplication in the frequency domain and defined in Eqn. 3.3 below. Then the Cepstral calculation follows:

$$Y(w) = X(w)H(w) \quad (3.3)$$

$$log\,|Y(w)| = log(|X(w)|\,.\,|H(w)|) \quad (3.4)$$

$$log\,|Y(w)| = log\,|X(w)| + log\,|H(w)| \quad (3.5)$$

$$\dot{Y}(w) = \dot{X}(w) + \dot{H}(w) \quad (3.6)$$

The received ultrasound echo signal y(t) can also presented as a convolution between the source function x(t) and a reflection function r(t) (the medium function) [67].

$$y(t) = x(t) * r(t) \quad (3.7)$$

The function used for reflections from a layered surface (assuming three layers) of the skin separated by a distance *d* can be written as

$$r(t) = R_1\delta(t) + R_2\delta(t - \frac{2d}{C}) \quad (3.8)$$

Rewriting $Eqn.\,3.8$ gives

$$r(t) = R_1\delta(t) + R_2\delta(t - \tau) \quad (3.9)$$

where $\sigma(t)$ is the Dirac delta function, C is the speed of sound, τ is the time of flight that replaces $\frac{2d}{C}$, R_1 and R_2 are the reflection coefficients of the layers and d is the thickness of the layers. In this thesis, while defining the layers, not only the reflection coefficient but also the transmission coefficient and the attenuation values are considered.

3.3 Wave Equation

The propagation of ultrasonic waves can be described using a second-order partial differential equation [35]**.**

$$P_{tt}(x,t) - C^2P_{xx}(x,t) = 0$$

$P_{tt}(x,t) = C^2 P_{xx}(x,t)$ *(3.10)*

where C is the speed of sound, $P(x,t)$ is pressure wave at given point and time and the subscripts designate partial derivatives.

The initial conditions are:

$P(x,0) = P_0(x)$, some initial displacement *(3.11)*

$P_t(x,0) = q_0(x)$, some initial velocity *(3.12)*

The above is simply the wave equation and its analytic solution could be written as a combination of forward and backward traveling waves as:

$P(x,t) = F(x+Ct) + G(x-Ct)$ *(3.13)*

Substituting the initial condition into$eqn\ (3.13)$we get:

$$P(x,0) = P_0(x) = F(x+0.t) + G(x-0.t)$$
$$= F(x) + G(x) \quad (3.14)$$

$$\frac{\partial P}{\partial t} = q_0(x) = F'(x+C.0)(C) + G'(x-C.0)(C)$$
$$= CF'(x) - CG'(x) \quad (3.15)$$

Integrate $eqn.(3.15)$ from x_0 to x:

$$\int_{x_0}^{x} q_0(s)ds = C(F(x) - F(x_0)) - C(G(x) - G(x_0))$$

$$\frac{1}{C}\int_{x_0}^{x} q_0(s)ds = F(x) - F(x_0) - [G(x) - G(x_0)]$$

$$\frac{1}{C}\int_{x_0}^{x} q_0(s)ds + F(x_0) - G(x_0) = F(x) - G(x) \quad (3.16)$$

Let's go through two more steps:

i. Add eqn 3.14 and 3.16

$$P(x,0) + \frac{1}{C}\int_{x_0}^{x} q_0(s)ds + F(x_0) - G(x_0) = F(x) + G(x) + F(x) - G(x)$$

$$P(x,0) + \frac{1}{C}\int_{x_0}^{x} q_0(s)ds + F(x_0) - G(x_0) = 2F(x) \quad (3.17)$$

Divide eqn 3.17 with 2 and replace x with $x + Ct$

$$\frac{1}{2}\left[P(x+Ct,0) + \frac{1}{C}\int_{x_0}^{x+Ct} q_0(s)ds + F(x_0) - G(x_0)\right] = F(x+Ct) \quad (3.18)$$

ii. Subtract eqn 3.14 and 3.16

$$P(x,0) - \frac{1}{C}\int_{x_0}^{x} q_0(s)ds - F(x_0) + G(x_0) = F(x) + G(x) - [F(x) - G(x)]$$

$$P(x,0) - \tfrac{1}{C}\textstyle\int_{x_0}^{x} q_0(s)ds - F(x_0) + G(x_0) = \ 2G(x) \tag{3.19}$$

Divide eqn 3.19 with 2 and replace x with $x - C$t

$$\tfrac{1}{2}[P(x - Ct, 0) - \tfrac{1}{C}\textstyle\int_{x_0}^{x-Ct} q_0(s)ds - F(x_0) + G(x_0)] = G(x - Ct) \tag{3.20}$$

Adding the forward and backward traveling waves from eqn 3.18 and 3.20:

$$\tfrac{1}{2}\ [P(\mathrm{x} + \mathrm{Ct}, 0) + \tfrac{1}{C}\textstyle\int_{x_0}^{x+Ct} q_0(s)ds + F(x_0) - G(x_0)] + \tfrac{1}{2}[P(x - Ct, 0) - \tfrac{1}{C}\textstyle\int_{x_0}^{x-Ct} q_0(s)ds - F(x_0) + G(x_0)] = G(x - Ct) + F(x + Ct)$$

$$\frac{1}{2}\ [P_0(\mathrm{x} + \mathrm{Ct}) + \frac{1}{C}\int_{x_0}^{x+Ct} q_0(s)ds] + \frac{1}{2}[P_0(\mathrm{x} - \mathrm{Ct}) - \frac{1}{C}\int_{x_0}^{x-Ct} q_0(s)ds = G(x - Ct) + F(x + Ct)$$

Now identify this equation as forward and backward traveling waves.

Backward traveling wave:

$$\tfrac{1}{2}\left[P_0(\mathrm{x} + \mathrm{Ct}) + \tfrac{1}{C}\textstyle\int_{x_0}^{x+Ct} q_0(s)ds\right] = \ F(x + Ct) \tag{3.21}$$

Forward traveling wave (P_f):

$$\tfrac{1}{2}[P_0(\mathrm{x} - \mathrm{Ct}) - \tfrac{1}{C}\textstyle\int_{x_0}^{x-Ct} q_0(s)ds = \ G(x - Ct) \tag{3.22}$$

In this thesis, the forward traveling ultrasonic wave (P_f) is taken into account. Accordingly, a forward traveling wave of a single frequency f_0 with corresponding angular frequency $\boldsymbol{\omega}$ and wave number $\boldsymbol{k}$ is assumed**.** The wave starts with an amplitude $A_0\ at\ (x,t) = (0,0)$. This phenomenon can be described as power law equation**.**

$$P_f(x,t) = A_0 e^{-j\omega(t-\frac{x}{C})} = A_0 e^{-j(\omega t - \frac{\omega}{C}x)} = A_0 e^{-j(\omega t - kx)} \tag{3.23}$$

In a real medium, acoustic attenuation by the medium occur which reduces the amplitude exponentially. Then the wave can be expressed as [35]. $P_f(x,t) = A_0.A(x,t)e^{-j(\omega t - kx)}$) where $A(x,t)$the ultrasound wave affected with attenuation [74].

$$A(x) = e^{-\dot{\alpha}x} \tag{3.24}$$

$$\dot{\alpha} = \alpha|f|^n \tag{3.25}$$

Here $\dot{\alpha}$ and n are material constants.

The solution to $eqn, 3.23$ in the positive x −direction, called the one-way wave equation [68] is given by:

$$P(x,w) = P(x_0,w)e^{-jk(x-x_0)}$$
$$= P(x_0,w)e^{-j\frac{w}{C}(x-x_0)-\alpha(x-x_0)} \tag{3.26}$$

In $e$qn. 3.26, the first part of the exponent ($\frac{x-x_0}{C}$) describes the time-of-flight and the second part the attenuation of the wave. The rate at which the amplitude of the wave is attenuating depends on the medium and the frequency of the wave. Attenuation is described as the exponential reduction of wave amplitude or intensity due to absorption, refraction and/or scattering. In soft tissues, however, attenuation due to scattering is negligible [39]. Also, since the refractive indices between the skin layers are minimal, the effect of attenuation due to refraction is neglected. In classical absorption theory, the attenuation coefficient can be approximated to be proportional to the square of the sound frequency, i.e., $\alpha(\omega) = \alpha\omega^2$ [74]. But in soft tissues, the dependence of ultrasound attenuation with frequency is almost linear and the square is omitted, i.e., $\alpha(\omega) = \alpha\omega$. The distance traveled by the wave is $d = x - x_0$ and defining the time-of-flight for a constant velocity as $\tau = (x - x_0)/C$, the collected exponential terms inside the i^{th} layer can be model as:

$$M_i = e^{-j\omega\tau_i - a_i\omega d_i} \tag{3.27}$$

3.4 Reflection and Transmission

A medium has a descriptive property in its acoustic impedance. For a low-loss medium, the acoustic impedance, measured in $Pa \cdot s/m$, can be written as $Z = \rho C$, where ρ is the density (kg/m^3) and *C* is the speed of sound (m/s).

The acoustic impedance is an important factor when describing the reflection and transmission of an incident wave at the tissue interfaces[39][69]. Assuming the incident wave to be perpendicular to the surface, the reflected and the transmitted waves connected to the incident wave are given as [74]:

$$Pref(x,w) = R_{k,l}Pinc(x,w) \quad (3.28)$$

$$Ptr(x,w) = T_{k,l}Pinc(x,w) \quad (3.29)$$

where $R_{k,l}$ is the reflection coefficient and $T_{k,l}$ is the transmission coefficient and the subscripts denote the two media.

The amount of the wave that is reflected and transmitted, respectively, depends on the acoustic properties of the two media, that is the sound velocities C_k and C_l and the densities ρ_k and ρ_l.

$$R_{k,l} = \frac{Z_l - Z_k}{Z_k + Z_l} \quad (3.30)$$

$$T_{k,l} = \frac{2Z_l}{Z_k + Z_l} \quad (3.31)$$

The quantities zl and zk are the acoustic impedances in the two media defined as $Z_k = \rho_k C_k$ where C_k is the speed of sound and ρ_k is the density in medium *k*.

3.5 Linear and Nonlinear Propagation

The system of propagation of the ultrasonic wave through a media is expressed mathematically as nonlinear. The degree of nonlinearity is dependent in media properties as well as media parameters described in acoustic wave propagation equations. According to previous studies [70][71],[74] the linear propagation of an acoustic wave means when an input source wave with specific amplitude is scaled, the resultant wave field is scaled by the same factor, and the acoustic wave equates to the superposition of the fields of the individual source waves. In the ideal case, i.e., a homogeneous lossless material, linear propagation of an acoustic wave with a specific amplitude and frequency should produce a waveform that retains the same shape and spectrum as the original source wave. For nonlinear acoustic wave propagation, the scaling and superposition principles no longer apply the effects of which manifest as the deformation of the pulse shape. The wave shape distortion is a function of propagation distance, selected resonant frequency and wave amplitude [70][54]. The ratio B/A is often used to determine the degree of non-linearity in a medium [70] where B and $A$are material properties. The truncation of the series to the first two terms (see Eqn. 3.32) is possible as the ratio *B/A* characterizes the dominant finite-amplitude contributions to the speed of sound in any fluid.

In this thesis, linear system is selected due the reason that the effect of nonlinearity index in soft tissue is small and periodic detection is no more achieved with nonlinear ultrasonic propagation system.

$$P = P_0 + A\left[\frac{\rho+\rho_0}{\rho}\right] + \frac{B}{2}[\frac{\rho+\rho_0}{\rho}]^2 + \cdots \quad (3.32)$$

3.5.1 Linear System

Ultrasonic measurement system is considered as a linear system in soft tissues. The generated signal is the input signal and the medium under investigation with its specific characteristics is the transfer function. The mathematical convolution of the two functions is the output or detected echo. The transfer function connects an input signal to an output signal [54][74].

When using transducer for practical case, the emitted signal from the transducer is unknown and the input to the system needs to be estimated. If the assumption of linear acoustics holds, there exists a linear system with impulse response $h(t)$ that describes the relationship between the output signal $y(t)$ and the input signal $u(t)$. However, when the source signal is simulated with estimated media function, the output signal is unknown [74]. The equation that describes how the transfer function $H(\omega)$ relates the output signal $Y(\omega)$ and the input signal $U(\omega)$is defined in the frequency domain as:

$$Y(w) = H(w)U(w) \quad (3.33)$$

where the capital letters denote Fourier-transformed quantities. If considering a wave traveling in a homogenous medium without boundaries, the transfer function is defined as:

$$\mathrm{H(w)} = \mathrm{M_i(w)} \quad (3.34)$$

where $\mathrm{M_i(w)}$is the model for the material properties inside the i^{th} layer as described in $eqn.\,3.27$ [39].

3.6 Input Signal

The estimation of the input signal is highly dependent on the measurement configuration (pulse-echo or through transmission), frequency of the transducer, and the medium under investigation. In this thesis, pulse echo configuration is used and US pulse is generated synthetically as an input signal. The transfer function on the other hand is estimated from the media parameters.

3.7 The Layer Model

Sending an ultrasonic pulse through a multi-layered material will produce output signal waveform consisting of several delayed and attenuated echoes. If the multi-layered structure has one or more thin layers, the signal waveform will consist of overlapping echoes. Several different solutions to handle multi-layered structures have been proposed [72], [74]. In this study, a system identification approach is used, where the multi-layered structure is described by a parametric model. The ultrasonic signal waveform is propagated through a multi-layered structure with four interfacing (reflectors). A system of linear equations has to be solved to derive the transfer functions between the defined input and output signals (See also Fig. 3.3).

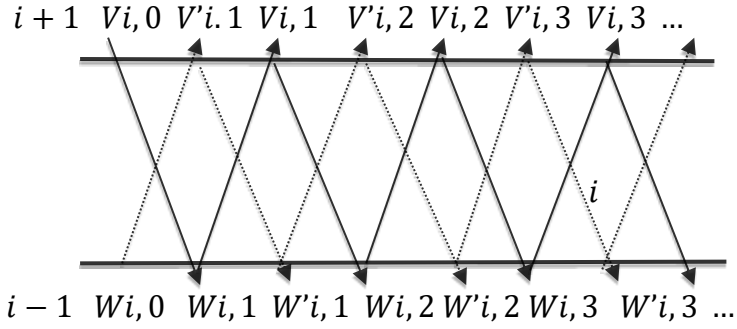

Figure 3.3 Single layer in a multi-layer structure:

$V_{i,0}$ represents the input signal from the layer above; $W_{i,0}$ represents the input signal from the layer below; $Vi,j,V'i,j,,Wi,j$, and $W'i,j$, for $j = 1,2,\dots,\infty$, represent the output echoes from the layer.

3.7.1. Single Layer in a Multi-Layered Structure

In a single layer inside a multi-layered structure, the input echoes to that layer are arriving from upper and lower boundaries. The following derivation considers input ultrasonic pulse and output echo from both boundaries and the omega notation is omitted to simplify the calculation. From Fig. 3.3., the input signal $V_{i,0}$ will contribute to the output echoes at both boundaries. Throughout this document i and j represent the number of layers and echoes and T and R are transmission and reflection coefficients, respectively [74].

The contributions at the upper boundary are

$$V_{i,1} = T_{i+1,i}R_{i,i-1}T_{i,i+1}M^2{}_iV_{i,0} \qquad (3.35)$$

Two transmissions exist between $i+1$ and i and one reflection from bottom boundary (between i and $i-1$).

$$V_{i,2} = R_{i,i-1}R_{i,i+1}M^2{}_iT_{i+1,i}R_{i,i-1}T_{i,i+1}M^2{}_iV_{i,0} \qquad (3.36)$$

$$V_{i,j} = R_{i,i-1}R_{i+1,i}M^2{}_iV_{i,j-1} \quad (3.37)$$

where$i$ and j indicate number of layers and echoes respectively.

$$V_{i,j} = \left(R_{i,i-1}R_{i,i+1}M^2{}_i\right)^{j-1}T_{i+1,i}R_{i,i-1}T_{i,i+1}M^2{}_iV_{i,0} \quad (3.38)$$

The input signal $W_{i,0}$ will also contribute to the output echoes at both boundaries. The j^{th}echo at the upperboundary created from this input can be written as

$$V'_{i,j} = \left(R_{i,i-1}R_{i+1,i}M^2i\right)^{j-1}T_{i+1,i}M_iV_{i,0} \quad (3.39)$$

The input signals will also produce output echoes at the lower boundary. The j^{th} echo at the lower boundary written as

$$W_{i,j} = T_{i+1,i}V_{i,0}\left(R_{i,i-1}R_{i+1,i}M^2i\right)^{j-1} \quad (3.40)$$

$$W'_{i,j} = R_{i+1,i}V_{i,0}\left(R_{i,i-1}R_{i+1,i}M^2i\right)^{j-1} \quad (3.41)$$

The upward output signal is the sum of all pressure waves leaving the i^{th} layer into the $(i+1)^{th}$ layer. This means that this output is the lower input signal $W_{i+1,0}$to the$(i+1)^{th}$ layer. Using the expressions in Eqn. (3.38) and (3.39), the upward output expressed as

$$W_{i+1,0} = \sum_{j=1}^{\infty}\left(V_{i,j} + V'_{i,j}\right) \quad (3.42)$$

$$= \frac{T_{i+1,i}R_{i,i-1}T_{i,i+1}M^2i(w)}{1 - R_{i,i-1}R_{i,i+1}M^2i(w)}V_{i,0} + \frac{T_{i,i+1}M^2i(w)}{1 - R_{i,i-1}R_{i,i+1}M^2i(w)}W_{i,0}$$

$$= A_iV_{i,0} + B_iW_{i,0} \quad (3.43)$$

where $\mathrm{A_i}$ and $\mathrm{B_i}$ are representation of the coefficients to $\mathrm{V_{i,0}}$ and $\mathrm{W_{i,0}}$ respectively.

From the geometrical progression,

$$\sum_{j=0}^{\infty}\left(x^j\right) = \frac{1}{1-x} \quad (3.44)$$

The downward output signal is the sum of all pressure waves leaving the ith layer into the $(i-1)^{th}$ layer. This means that this output is the upper input signal $V_{i-1,0}$ to the $(i-1)^{th}$ layer. The downward output can be expressed as

$$V_{i-1,0} = \sum_{j=1}^{\infty}\left(W_{i,j} + W'_{i,j}\right) \quad (3.45)$$

$$= \frac{Ti+1,iMi(\mathrm{w})}{1 - \mathrm{Ri,i-1Ri,i+1}M^2i(\mathrm{w})}V_{i,0} + \frac{Ri,i+1M^2i(\mathrm{w})}{1 - R_{i,i-1}\mathrm{Ri,i+1}M^2i(\mathrm{w})}W_{i,0}$$

$$= C_iV_{i,0} + D_iW_{i,0} \quad (3.46)$$

where, C_i and D_i are representation of the coefficients to $V_{i,0}$ and $W_{i,0}$ respectively.

The expression in $eqn\ (3.43)$ *and* (3.44) can be written using the relationship $T_{i,j}$=1+$R_{i,j}$ and $R_{i,j} = -R_{j,i}$ (T and R represents reflection and transmission coefficients):

$$Ai = \frac{(1-R^2i+1,i)Ri,i-1M^2i(\mathrm{w}}{1+\mathrm{Ri,i-1Ri,i+1}M^2i(\mathrm{w})} \quad (3.47)$$

$$Bi = \frac{(1-\mathrm{R}i+1,i)Mi(\mathrm{w})}{1+\mathrm{Ri,i-1Ri,i+1}M^2i(\mathrm{w})} \quad (3.48)$$

$$Ci = \frac{(1+Ri+1,i)Mi(\mathrm{w})}{1+\mathrm{Ri,i-1Ri,i+1}M^2i(\mathrm{w})} \quad (3.49)$$

$$Di = \frac{Ri+1,iM^2i(\mathrm{w})}{1+\mathrm{Ri,i-1Ri,i+1}M^2i(\mathrm{w})} \quad (3.50)$$

By using $eqn\ (3.43)-\ eqn\ (3.50)$, the appropriate model for a multi-layered structure with an arbitrary number of layers, j, can be found. The model can be derived with input- and output signals above and/or under the material; that is, pulse-echo or through-transmission configuration in both directions and both jointly.

3.7.2. One-Layered Structure ($\boldsymbol{j = 1}$)

In a pulse-echo configuration with input and output signal above the material$V_{1,0}$is the input signal and $W_{1,0}$ is zero. The model for $I = 1$, using the knowledge that the input from the layers below is zero, $W_{1,0} = 0$.

$$W_{2,0} = A_1V_{1,0} + B_1W_{1,0} \quad (3.51)$$

$$= A_1V_{1,0} \quad (3.52)$$

This equation gives us the model for a pulse-echo configuration with input and output signal above the material

$$H_1(w) = A_1(w) \quad (3.53)$$

$$= \frac{(1-R^221)\mathrm{R}10M^21(\mathrm{w})}{1+\mathrm{R}10\mathrm{R}21M^21(\mathrm{w})} \quad (3.54)$$

where $M1(\omega)$ is the collected material properties in the single layer defined $in\ eqn.3.27$. This is the model for a one-layer structure in pulse-echo configuration with transmitter and receiver above the material. For a one-layer structure, the total model can be stated using a system of linear equations in a block matrix form as:

$$\begin{bmatrix} W_{2,0} \\ V_{0,0} \end{bmatrix} = \begin{bmatrix} A_1 & B_1 \\ C_1 & D_1 \end{bmatrix} \begin{bmatrix} V_{1,0} \\ W_{1,0} \end{bmatrix} \quad (3.55)$$

where the different choices of input and output signals give the desired model. Observe that when removing the second row and column in the matrix, the model for the pulse-echo configuration is achieved. A similar matrix of linear equations can be built up, extending the

model for two, three and more layers. The 0 in the input signals $V_{i,0}$ and $W_{i,0}$, denotes that the total output from layer *q* at the upper boundary is defined as the first echo in layer $(i + 1)$, denoted $W_{1,0}$. The upward output signal is the sum of all pressure waves leaving thei^{th} layer into the $(i + 1)th$ layer. This means that this output is the lower input signal $W_{i+1,0}$ to the $(i + 1)th$ layer.

3.7.3. Two-Layered Structure

The model for a medium with two layers, $I = 2$, is found using the same approach as for a medium with one layer, by examining the reflections of the input signal from inside the medium. A matrix can be found for the 2-layered structure by expanding for another layer.

$$\begin{bmatrix} W_{3,0} \\ V_{1,0} \\ W_{2,0} \\ V_{0,0} \end{bmatrix} = \begin{bmatrix} A_2 & B_2 & 0 & 0 \\ C_2 & D_2 & 0 & 0 \\ 0 & 0 & A_1 & B_1 \\ 0 & 0 & C_1 & D_1 \end{bmatrix} \begin{bmatrix} V_{2,0} \\ W_{2,0} \\ V_{1,0} \\ W_{1,0} \end{bmatrix} \qquad (3.56)$$

In a pulse-echo configuration with input and output signals above the material, $V_{2,0}$ is the input signal and $W_{1,0}$ is zero. The output signal $V_{0,0}$ is not interesting, and $W_{3,0}$ is the interesting output signal. The reflected waves give rise to additional reflected echoes. All these reverberations are included in the model and rapidly complicate it. By using the knowledge of a pulse-echo configuration, the system of linear equations reduces to

$$\begin{bmatrix} W_{3,0} \\ V_{1,0} \\ W_{2,0} \end{bmatrix} = \begin{bmatrix} A_2 & B_2 & 0 \\ C_2 & D_2 & 0 \\ 0 & 0 & A_1 \end{bmatrix} \begin{bmatrix} V_{2,0} \\ W_{2,0} \\ V_{1,0} \end{bmatrix} \qquad (3.57)$$

The signals $V_{1,0}$and $W_{2,0}$ are the input and output at the middle interface between thefirst and second layers, respectively. These signals are used in the calculations and guarantee that all reverberations are taken into account as they include the terms A_1 , B_2 , C_2 , and D_2 in the model, which contain the internal reverberations, see $Eqn.\,(47)-(50)$. Solving this system of linear equations with respect to the output and input signals will give us the model for a 2-layered structure. The linear equations are:

$$W_{3,0} = A_2\, V_{2,0} + B_2\, W_{2,0} \qquad (3.58)$$

$$V_{1,0} = C_2\, V_{2,0} + D_2\, W_{2,0} \qquad (3.59)$$

$$W_{2,0} = A_1\, V_{1,0} \qquad (3.60)$$

To find the output signal $W_{3,0}$expressed in the input signal $V_{2,0}$, we insert *eqn.* (3.59) into e*qn.* (3.60) and solve for $W_{2,0}$, we insert the result into *eqn.* (3.58), and the result is

$$W_{3,0} = A_2\, V_{2,0} + B_2\, \frac{C_2\ A_1}{1-D_1\ A_1} V_{2,0}) \quad (3.61)$$

where A_{i} , $B_{2\,\mathrm{i}}$, C_{i} and D_{i} represents the coefficients of $V_{i,\mathrm{j}}$and $W_{i,\mathrm{j}}$as it is defined in $eqn.\,3.47$ to 3.50. This equation gives us the model for a pulse-echo configuration with both input and output signals above the material

$$H2(w) = A_2 + B_2\, \frac{C_2\ B_2\ A_1}{1-D_1\ A_1} \quad (3.62)$$

3.7.4. Recursive Solution to Model Transfer Function

In pulse echo configuration, both the input and output are on the top of the layer and the bottom layers are missing. A single transducer served as a transmitter and receiver above the structure. Previous studies [74], [75] showed that it is possible to find a recursive expression for the model in pulse echo configuration. The expression for transfer function for "I" layers found using the recursive expression is given by:

$$Hi = \begin{cases} A_{\mathrm{i}} + \frac{C_{\mathrm{i}}\ B_{\mathrm{i}}\ H_{i-1}}{1-D_{\mathrm{i}}\ H_{i-1}}, & i > 1 \\ A_1\ , & i = 1 \end{cases} \quad (3.63)$$

3.8. The Multi-Layered Model

In ultrasonic measurements, the received ultrasonic echoes are evaluated to retrieve information about the inspected media. The information extracted from the media varies depending on the characteristics of the media under inspection. The appropriate parametric model of received echo is required to find the ultrasonic waveform [27], [76], [77]. The studies focus on modeling the media under investigation with a parametric model, estimation of the parameters of that model, and on the analysis of the model parameters.

The current thesis study examines ultrasonic waves with normal incidence, media with multi-layered structures and thin layers. Instead of modeling the individual echoes in the waveform, the layered model is considered with its appropriate parametric values. A received waveform consisting of several reverberant and overlapping echoes is considered when dealing with thin layers. A parametrization of the layers that is related to physical properties of the investigated materials structure instead of each echo is preferable.

The thickness of the thinnest layer is in the order of the wavelength of the ultrasonic wave in that layer, creating a response signal consisting of overlapping waveforms. Increasing the US pulse frequency and decreasing the pulse width is often the usual approach to prevent

overlaps [78]. A pictorial representation of the four layered model proposed in this thesis is shown in Fig. 3.4. The layered model in Fig. 3.4 entails how ultrasonic wave is transmitted and reflected in a multilayered media. On the figure the ultrasonic pulse is made incident obliquely to show how the waves are transmitted and reflected in a multilayered media. Otherwise, the current thesis work considers only normal ultrasonic incidences.

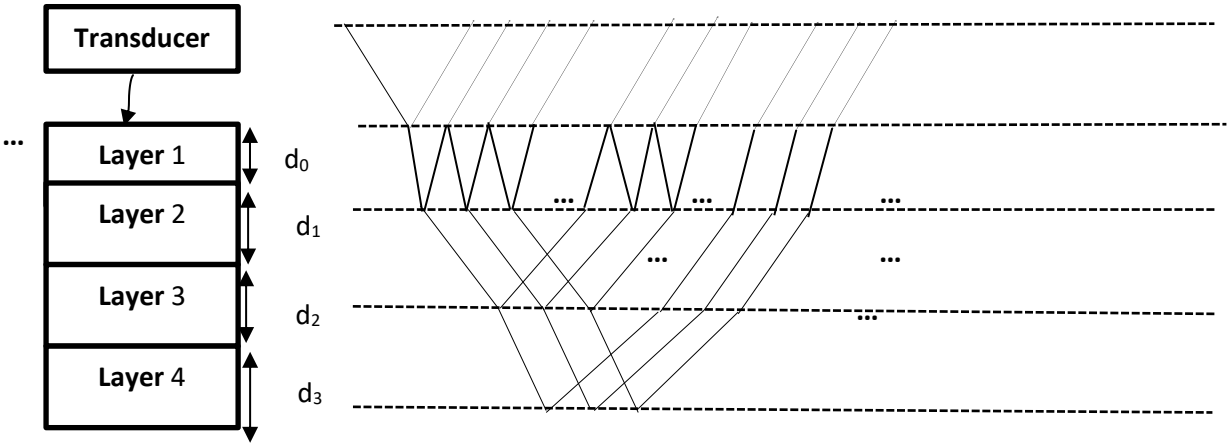

Figure 3.4 Four layered model.

3.9 Periodicity Detection

A period is defined as the smallest specified time interval between successive points in a repeating waveform. The periodicity of ultrasonic echo can be detected analytically or/and numerically.

3.9.1 Analytically

$$x(t) = x(t+T) \qquad \forall t, \text{where } T > 0 \qquad (3.64)$$

where *T* represents the specified time interval in essence the period [5]. In order to gather diagnostic information about the various layers in the biological layered tissue, an ultrasonic source wave is transmitted to the skin and the subsequent echoes and reverberations assessed. In the event that no deviations or appreciable anomalies exist in the layers, the produced echoes and reverberation are expected to exhibit a quasi-periodic nature [14].

3.9.2 Numerically

Considering the relative proximity of the individual consecutive skin layers in the layered structure, the generated echoes produced will interact in such a fashion where direct separation of individual echoes associated with particular layers will be indistinguishable [18].

The interaction of US pulse in multilayered medium results in overlapping echoes. In this project, the separation technique that employed Cepstrum analysis is used as a numerical technique. The implementation is shown entirely on a MATLAB platform. The resultant echo $y(t)$ is given by the convolution of the ultrasonic input signal $x(t)$ and the layered structure $h(t)$:

$$y(t) = x(t) * h(t) \tag{3.65}$$

Taking the Fourier Transform of Eqn. 3.65 and taking the magnitude gives the equivalent frequency domain representation:

$$|Y(w)| = |X(w)||H(w)| \tag{3.66}$$

Taking the logarithmic magnitude of Eqn. 3.66 results in:

$$\log|Y(w)| = \log|X(w)| + \log|H(w)| = Ys \tag{3.67}$$

The cepstrum ultimately obtained by taking the inverse Fourier Transform of $eqn\ 3.67$.

$$ys[n] = F^{-1}(Ys) \tag{3.68}$$

Taking the Cepstrum of the resultant echo will reveal pertinent information about how the number of layers, the distance between layers and the medium properties affect the periodicity of the resultant echo. The periodicity of the resultant echo can be detected in two ways. One is with consecutive peaks or ‘spikes’ that will be observed at equal or integer multiples of the smallest difference in time of the peak amplitude. The integer relationship between the peaks in the Cepstrum plot is indicative of periodicity in the resultant echo. The second method involves observing the log magnitude spectra [9].

Chapter 4. Research Methodology

The propagation of US pulse through biological tissues produces reflection, transmission and attenuation upon interaction. The reflected signal is the very important signal to form US images. This signal is designed to reside in the time domain and transformed to the frequency domain using Fourier transform and Cepstrum for periodic analysis. In the Cepstrum analysis, the periodicity of the wideband US signal is analyzed for different bandwidths, pulse widths, and center frequencies. In this thesis, the reflection, transmission and attenuation coefficients of the media were taken into account. The general idea of the proposed approach to meet the research objectives is flowcharted in Fig 4.1.

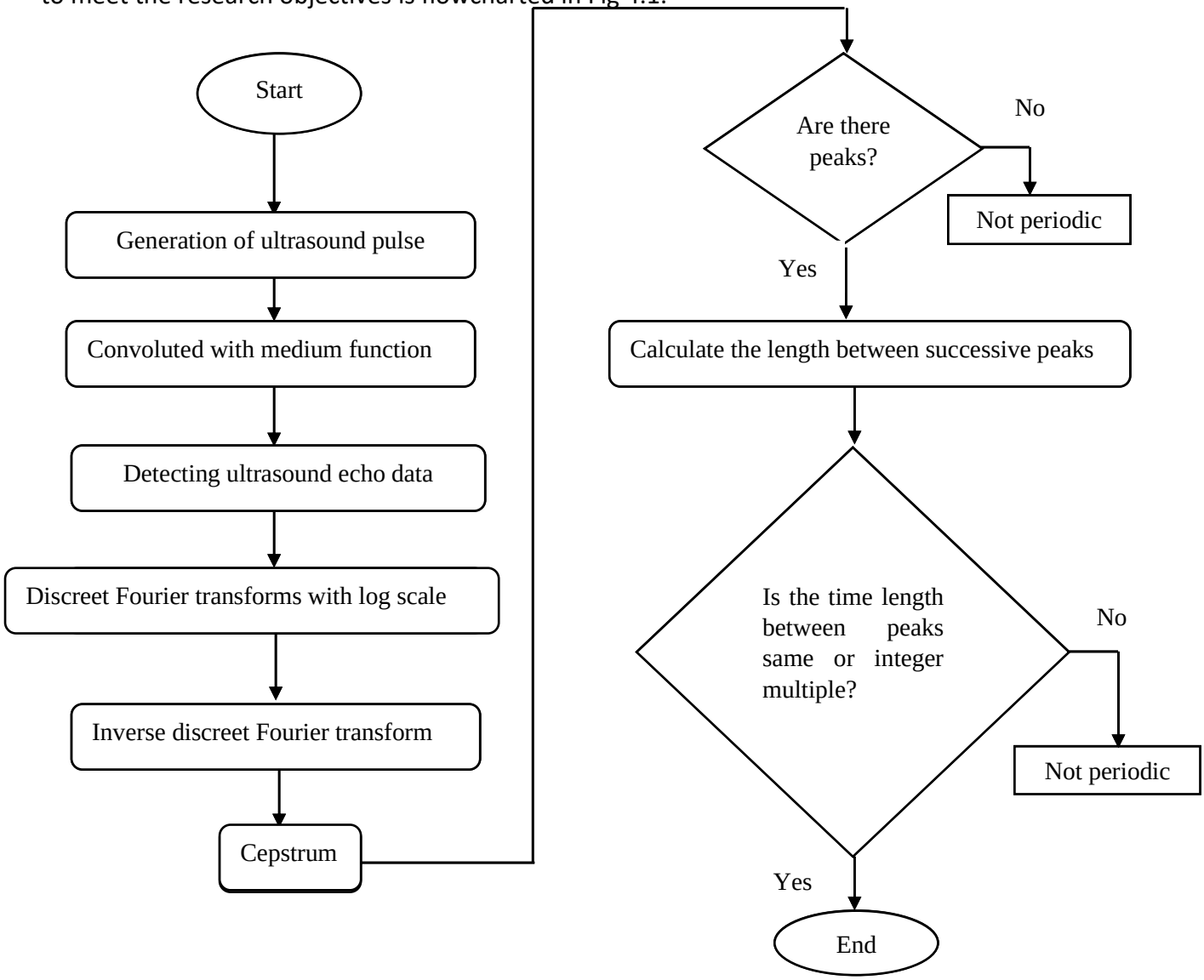

Figure 4.1 An overview of the system to detect periodicity.

The basic signal processing required to detect periodicity will be concerned with

- Detecting time domain echoed pulses.
- Converting to the frequency domain.
- Applying discrete Fourier Transform (FFT) to the logarithm function.
- Applying the inverse-discrete Fourier transform to the log FFT.

The components making up the periodicity detection process are shown in Fig. 4.2 below.

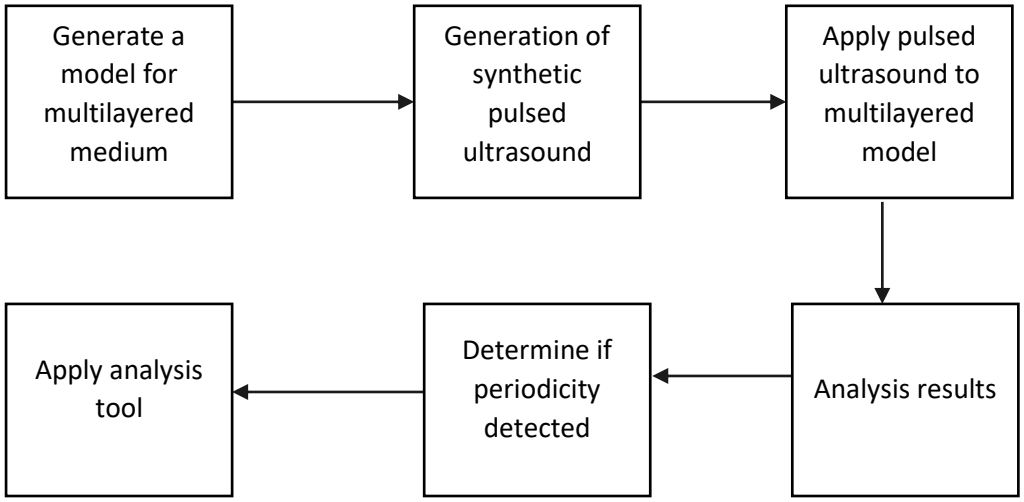

Figure 4.2 Overview of the proposed periodicity detection system.

4.1 Synthetic Pulsed Ultrasound Generation

Ultrasound pulse is generated synthetically by considering the pulse parameters suitable for diagnostic application. A rectangular modulated sinusoidal pulse waveform is used as the synthetic US pulse. Rectangular modulated sinusoid pulse is chosen as it is a wide bandwidth signal in the frequency domain and it has the ability to excite a large number of frequency components of the LTI system. The application of pulsed US wave to the multi-layered model and the feasibility of detecting periodicity in this medium is investigated in this thesis project [14].

Frequencies between 16 to 30 MHz are selected for this thesis work because this frequency range is commonly used for medical diagnosis on the superficial level. The pulse duration of 0.12 microseconds and 0.8 microseconds are used to generate the source signal.

The pulse duration and wavelength in the input signal are less than the time of flight of the thinnest layer and the length of the thinnest/smallest layer respectively. If these conditions are not met, then the input signal is no longer considered as a pulse.

The Cepstral peak can be exhibited at the integer multiples of Δt, doubling the ratio of thinnest tissue layer (d) to speed of sound (C). The term Δt is the smallest time of flight difference between tissue layers under investigation. On the Cepstral plot, the successive echoes are represented by a single peak located at positions Δt, and at multiples ofΔt. The value of Δt may be determined from the position of the peak of the maximum amplitude or from the distance between the peaks.

4.2 Signal Processing

The output signal (convolution of source and medium function) represents the response of an US signal having propagated through the multi-layered media. This signal is then converted to its frequency-domain equivalent $Y(\omega)$ through the application of the discreet Fourier transform (DFT). The resulting log scale Discreet Fourier transform under goes inverse Fourier transform and cepstrum is applied. Once cepstral approach is applied the existence of cepstral peaks and the time difference between each peak is examined. The process of Cepstral analysis can be applied as depicted in Fig. 4.4:

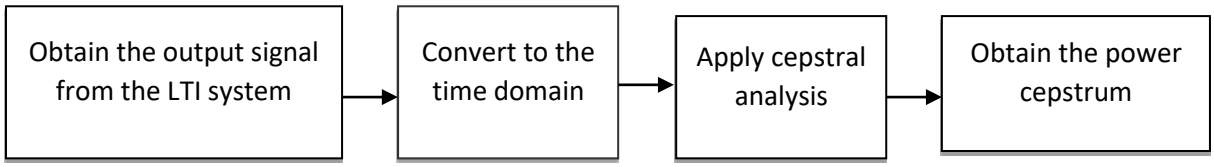

Figure 4.3 Signal Processing

- Detecting the time domain echoes pulses
- Converting to the discrete frequency domain
- Applying the logarithm function to results
- Applying the inverse Fourier-Discrete transform

The most commonly used Cepstral analysis methods are Power Cepstrum and the Complex Cepstrum. The complex Cepstrum inherently retains the phase information of the composite data sequence. This is very advantageous, as the complex Cepstrum will display peaks at echo arrival times and it is possible to fully recover the basic wavelet as the phase information is retained, but this requires phase unwrapping processes. The power Cepstrum is only used to

analyze what happens when the US beam is propagated through the medium irrespective of recovering the original signal as it is not required to obtain the basic signal waveform.

4.3 Signal Analysis

The output signal produced from applying Cepstral analysis is analyzed according to procedures shown Fig. 4.5 below. The main component involved in the signal processing is the peak detection algorithm which aims to processes real Cepstrum which can help determine pertinent information related to the detection of periodicity or the ability to detect multiple layers. The details regarding the development of the tool can be found in previous literature [10]. The tool aims to compute the distance between peaks in the Cepstrum.

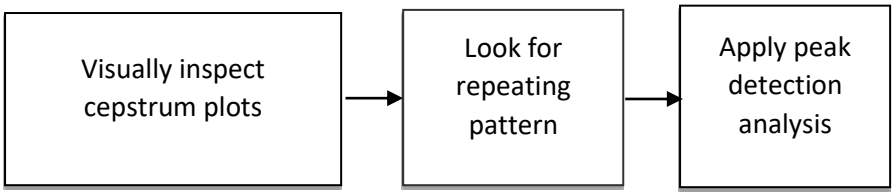

Figure 4.4 Signal Analysis general procedures

4.4 Testing Parameters

Layers of the human skin (including blood within) are considered in this thesis as multilayered biological medium to investigate the feasibility of detecting periodicity with wideband ultrasonic pulse. The multilayered medium under investigation is the human skin tissue that consists of four layers epidermis, sub layers of dermis, hypodermis and the blood. The density, thickness, acoustic impedance, propagation speed, and attenuation coefficient of these layers are defined in Table 4.1.

Table 4.1 Tissue layers with their parametric values

Layers	**Propagation speed (m/s)**	**Density (kg/m³)**	**Acoustic impedance (MRayl)**	**Thickness (mm)**	**Attenuation coefficients @1Mhz**
Epidermis	1645	1033	1.64	0.1	0.440dB/cm
Papillary	1595	1048	1.70	0.8	0.352dB/cm
Reticular	1488	1055	1.57	0.6	0.237dB/cm
Hypodermis	1450	1172	1.34	1-5	0.312dB/cm
Blood	1520	1060	1.61	1-3	0.140dB/cm

C.Moran,1995 and T. Szabo, 2013

Five layers (four boundaries) were chosen considering two cases. Case one with the same layers thickness ($0.3mm$) and the second with different layers thicknesses (0.1mm, 0.8mm, 0.6mm, 1mm). The reflection coefficient, transmission coefficient and attenuation of each layer are taken from Table 4.1. These data are used in generating the synthetic ultrasonic pulses. In generating the echoes, different reflection and transmission coefficients were taken. The time of flight in both cases is calculated from the thickness of the layers $\left(\tau = \frac{2d}{C}\right)$. Also, the minimum time of flight is calculated from the thinnest layer thickness ($0.4\mu \sec$ and $0.2\mu\ sec$) in same and different layer thickness, respectively.

Chapter 5. Results and Discussion

5.1 Introduction

The thesis was designed aiming at determining the possibility of detecting periodicity in a multi layered biological media by generating synthetic wideband US pulse. The results displayed in this chapter include the generated US pulse, its convolution with the media function or impulse response, its Fourier transform of the convoluted pulse in log scale, and the Cepstrum.

5.2 Results

The purpose this thesis was to generate/simulate synthetic ultrasonic pulse with reasonable pulse parameters and determine the detection of periodicity in multilayered biological media and determine the range bandwidths (if any) at which periodicity occurs. The technique used to illustrate the phenomenon is Cepstral analysis, as discussed in the methodology section presented in the previous chapter.

Results showed that the two-layered (one interface) media shows one dominant peak, whereas the plots for three, four and five layers (two, three and four interfaces) show multiple peaks at regular intervals (at equal or integer multiples of the fundamental peaks). The fundamental peak is determined from the smallest time of flight. The smallest time of flight is also calculated from the thinnest layer. In the case of two layered (one interface) medium, one dominant peak is plotted and the periodicity of the propagated signal could not be decided. However, in medium with more than two layers, it was easy to detect periodicity. That means for medium with more than two layers, the Cepstral peaks occurred at integer multiples of the fundamental peaks indicating periodicity. This confirms that the Cepstrum approach is detecting periodicity of wideband US over multilayered skin media. However, the number of layers cannot be distinguished from the Cepstral approach, extra information that could be of great importance.

5.2.1 Generating Synthetic Ultrasound Pulse

Rectangular pulse with pulse durations of 1.2×10^{-7} seconds and 0.8×10^{-7} seconds, minimum time of flight (TOF) of 0.4 and 0.2 seconds were generated with corresponding bandwidths of 8 MHz and 13 MHz, respectively. These values tell the inverse relationship between the pulse duration and bandwidth. Spike of pulse produce wideband spectrum and wider pulse produce

narrower bandwidth. The pulse duration and TOF values were assumed to be realistic for ultrasound pulse generation [72]. Figure 5.1 shows the two pulses generated in the time domain with their corresponding frequency domain spectra. The negative time vector entails that the time vector to generate the pulse is taken from its negative time points too*(-3.2x10^{-6} to +3.2x10^{-6}).*In Fig. 5.1 the bandwidths are calculated from -6dB (half) of the maximum wave amplitude.

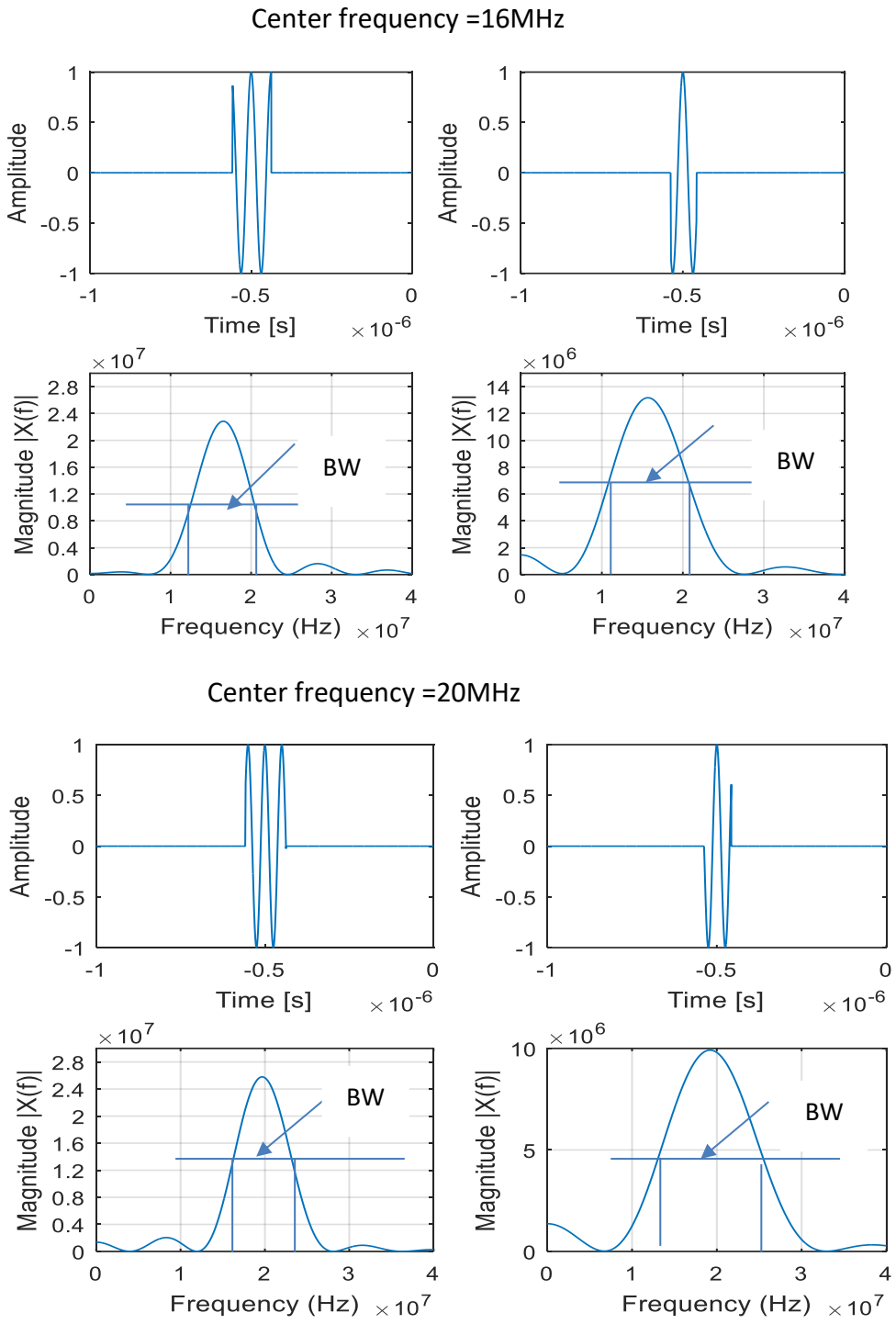

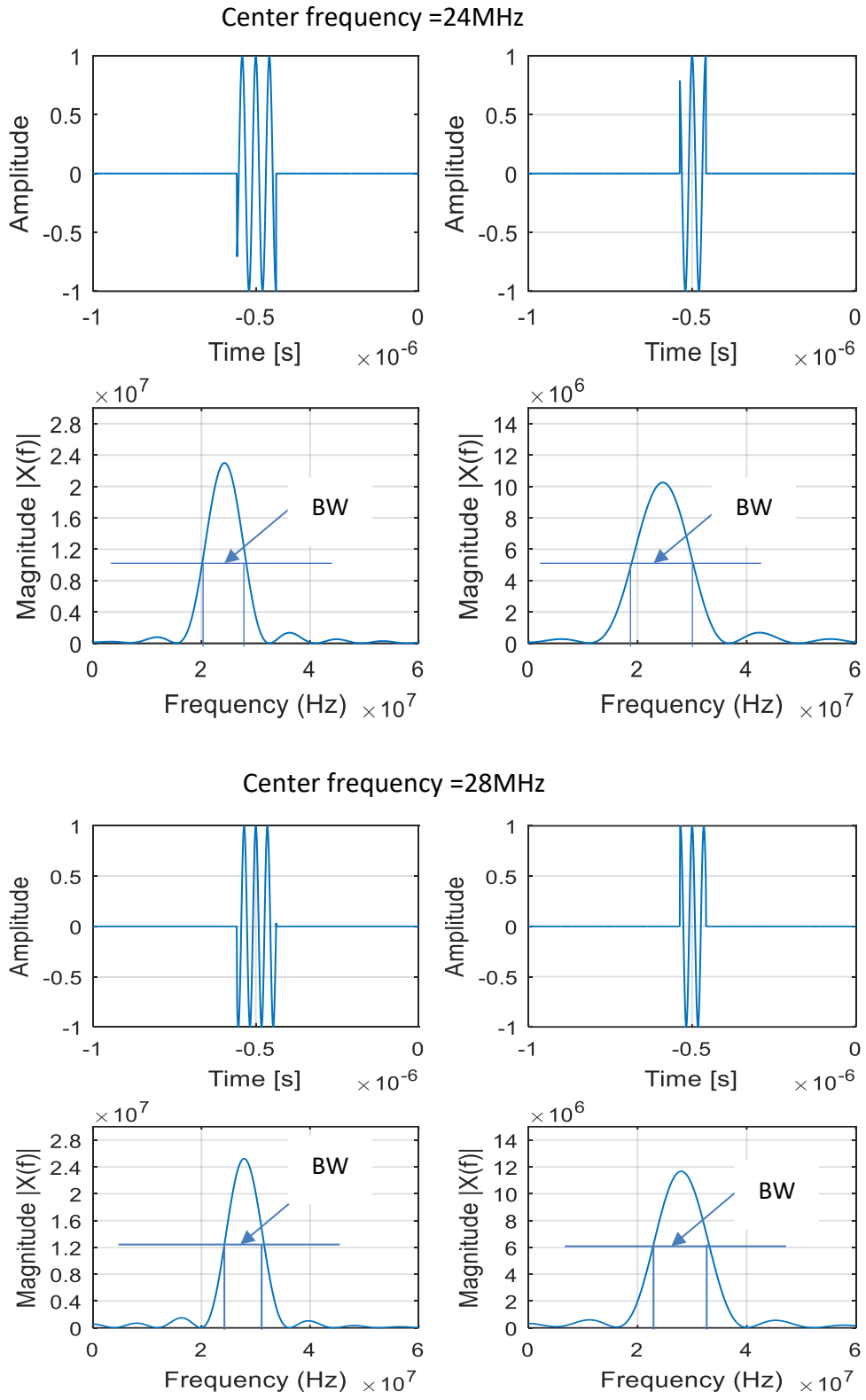

Figure 5.1 Synthetically generated ultrasound pulses and corresponding frequency domain at different center frequencies:

pulse duration = $1.2\text{x}10^{-7}$ sec(left), pulse duration = $0.8\text{x}10^{-7}sec$(right).

5.2.2 Detecting the Echoes at Different Interfaces

Echo is detected at the interfaces of the tissue and the amplitude of the echo detected depends primarily on the acoustic impedance mismatch between the interfacing layers. Mathematically echo can be detected with the convolution of the source function and the medium function. Fig. 5.2 presents the echoes generated this way assuming the same layer depths while Fig. 5.3 presents the echoes assuming variable layer depths.

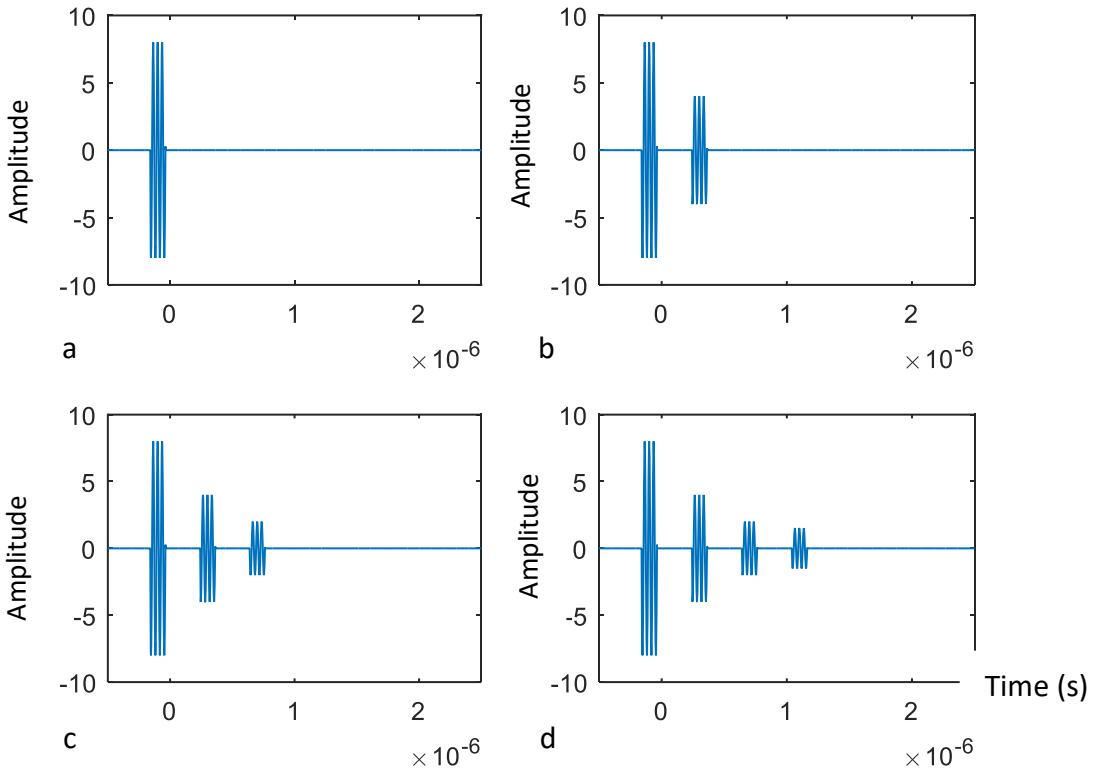

Figure 5.2. Detected echoes assuming same layer thickness:

(a) Detected echo for one layer, (b) Detected echoes for two layers,
(c) Detected echoes for three layers and (d) Detected echoes for four layers.

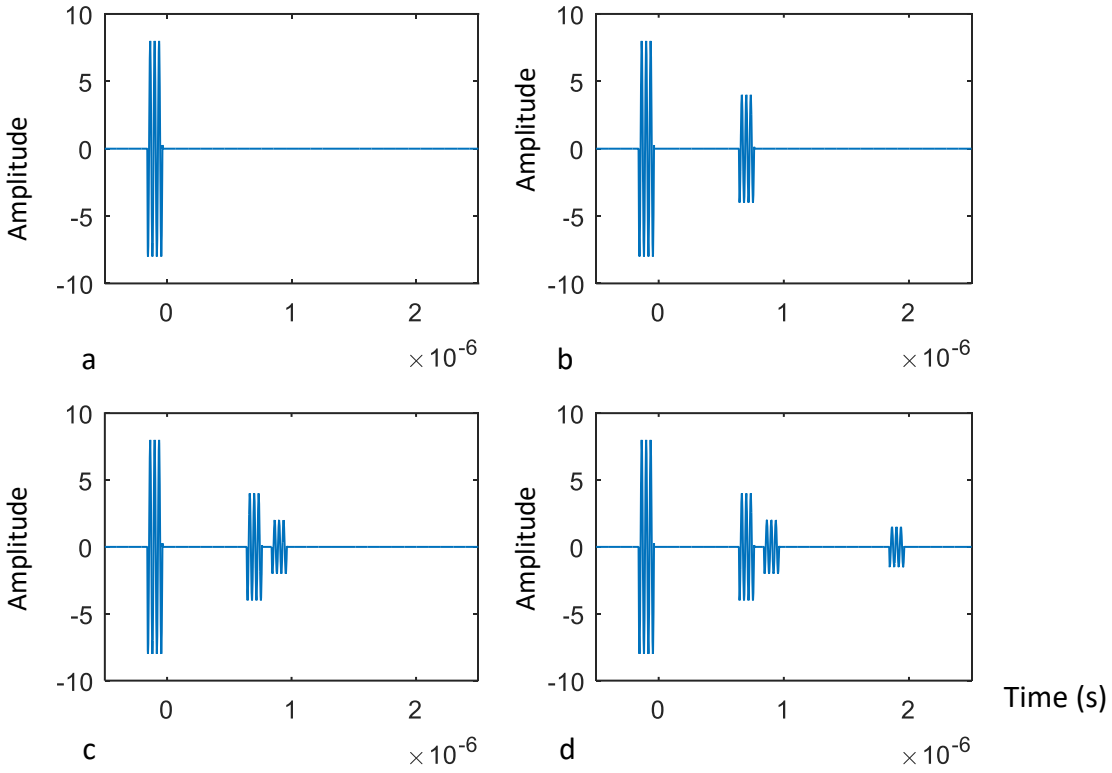

Figure 5.3 Detected echoes with different layer thickness:

(a) Detected echo for one layer, (b) Detected echoes for two layers,
(c) Detected echoes for three layers and (d) Detected echoes four layers.

5.2.3 Logarithmic Scale Amplitude Spectrum

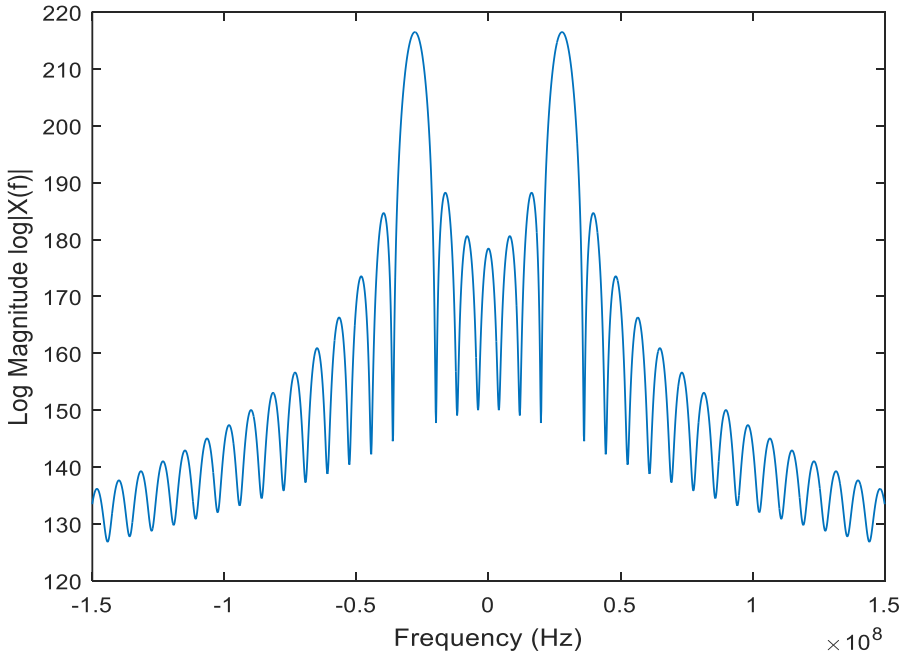

Figure 5.4 Corresponding logarithmic scale of fast Fourier transform (scalloping).

Fig. 5.4 presents the log scale Fourier amplitude spectrum of the echo generated in Fig. 5.2 (a). We could see from the figure that the maximum amplitude is attained at the center frequency of the generated ultrasonic pulse and there is a monotonically decreasing pattern generated as we go further away from the center frequency.

5.2.4 Cepstral Peaks

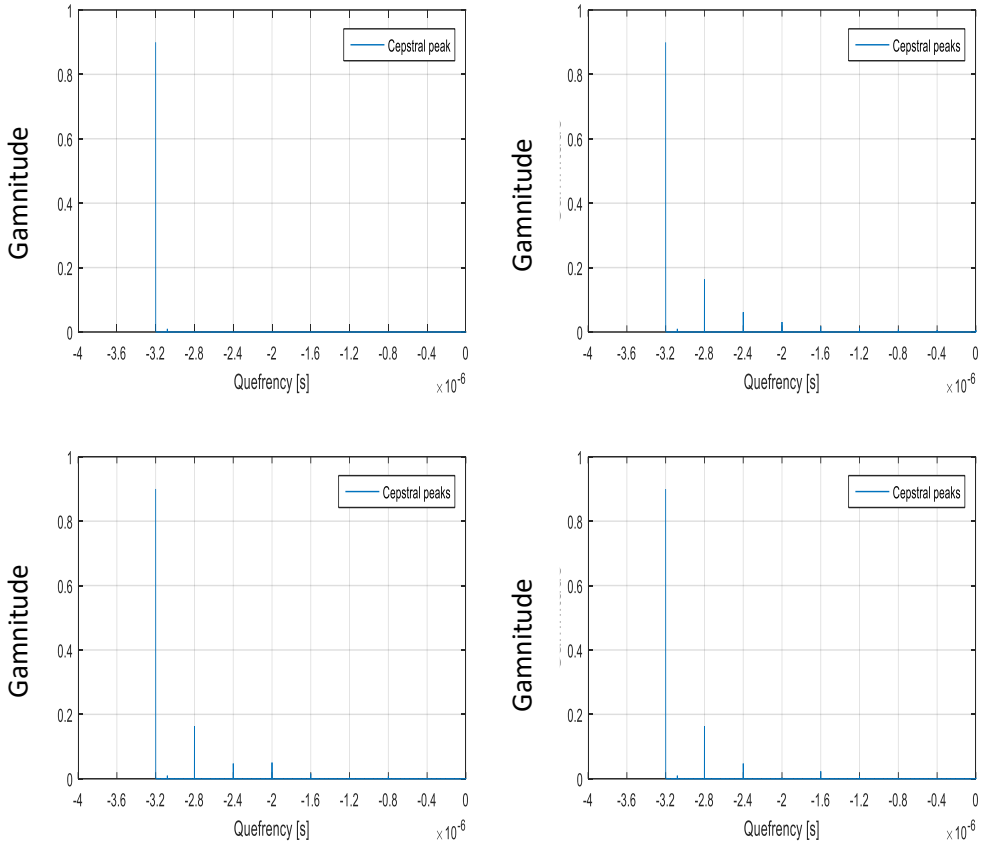

Figure 5.5 Detected cepstral peaks:

One layer (top left), Two layers (top right),
Three layers (bottom left) and Four layers (bottom right).

Fig. 5.5 presents the Cepstral peaks detected for medium with different number of layers assuming same thickness. In the case of layers separated by equal thickness ($0.3mm$ of each with time of flight of $0.4\mu sec$), the Cepstral peaks are existed at equal intervals of 0.4 microseconds. This pattern of Cepstral peaks existence entails the detection of periodicity. The negative sign in the horizontal axis (quefrency) is the one side of the cepstral pattern. The plot of Cepstrum is symmetric as it is in Fourier spectrum.

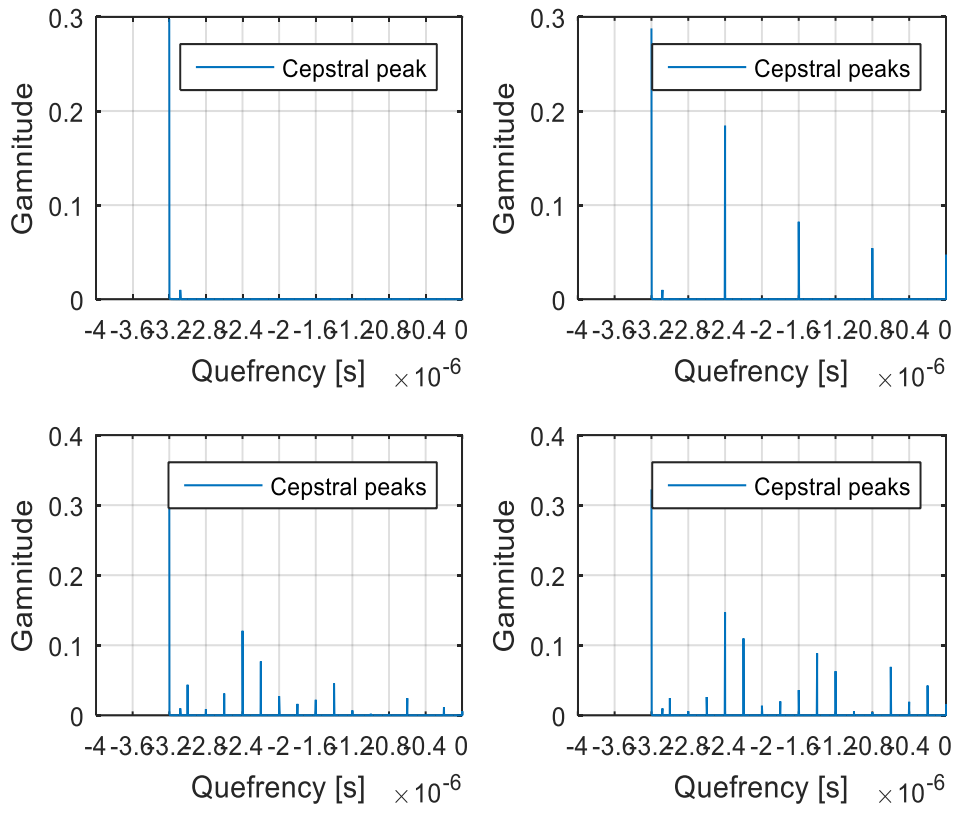

Figure 5.6 Detected echoes where layers with different thickness:

One layer (top left), Two layers (top right),
Three layers (bottom left), Four layers (bottom right).

In the case of layers separated with different layer thickness, as shown in Fig. 5.6, the dominant Cepstral peaks exist at integer multiples of the fundamental peak (that is 0.2 microseconds in the Fig. 5.6). This value of the time of flight is the time taken for the thinnest layer in the medium. One of the important considerations in Cepstral analysis is to know the effects of the pulse duration. Table 5.1 presents the effects of the pule duration on bandwidth and axial resolution of ultrasound image mathematically.

Table 5.1 The effect of pulse duration on bandwidth and axial resolution.

Center frequency	Pulse duration	Max frequency	Min frequency	Bandwidth	Axial resolution
$16\ MHz$	0.12µsec	20	12	8 MHz	0.0965 mm
	0.08 µsec	21	11	10 MHz	0.07 mm
$20\ MHz$	0.12 µsec	24	16	8 MHz	0.0965 mm
	0.08 µsec	25	13	12 MHz	0.064 mm
$24\ MHz$	0.12 µsec	28	20	8 MHz	0.0965 mm
	0.08 µsec	30	18	12 MHz	0.064 mm
$28\ MHz$	0.12 µsec	32	24	8 MHz	0.0965 mm
	0.08 µsec	34	22	12 MHz	0.064 mm

Table 5.1 explains the relation between the pulse width, bandwidth and axial resolution of ultrasonic image. When a small pulse width is used in time domain wide band width in frequency domain and this finally produces better axial resolution.

5.3 Discussion

We investigated in Fig 5.1 the US bandwidth in relation to the corresponding pulse durations, the Cepstral plots and periodicity. The bandwidth investigation showed that the largest difference in bandwidths is $12\ MHz$ when the pulse duration is $0.08\mu sec$ and the minimum bandwidth is $8\ MHz$ when the pulse duration is 0.12 μsec. The maximum and minimum bandwidths are determined from the content of the pulse duration. The minimum pulse duration in turn is governed by the minimum time-of-flight. Hence, the minimum bandwidth is governed by the maximum time-of-flight. That means layers with larger time-of-flight values will require smaller bandwidths for determination of periodicity. In addition, the thinnest layer determines the ultrasonic wavelength and this limits the center frequency. The smallest time of flight is also calculated from the thinnest layer and the speed of US in the medium. The minimum center frequency in this thesis is about $16\ MHZ$. Moreover, the thickness of the layers for a medium with equidistant layers and the smallest layer thickness for medium with variable layer thickness can be calculated from the Cepstral plots. In the case of periodicity detection, there is a noticeable trend in the Cepstral peaks as the number of layers increases from two to four. The trend observed is that the Cepstral peaks existed at equal time difference or integer multiples of the smallest time of flight.

Chapter 6. Conclusion and Recommendation

6.1 Conclusion

The current thesis was focused on the detection of periodicity of wideband US in multilayered biological media using the approach of Cepstral analysis. To do this, we have considered two scenarios: one assumes equidistant layers and the other is layers with different layer thicknesses. When considering layers with different thickness, it can be observed that peaks are existed at integer multiples of the smallest distance that is measured in seconds. It can be concluded that for more than two layers, the wideband US with equal distances, the peaks are existed at equal intervals, again verifying periodicity. The minimum bandwidth is governed by the pulse duration, which is governed by the minimum time-of-flight in the layers.

No sufficient research works have been done in the area of US based Cepstral analysis for biomedical engineering applications. This made the current thesis work challenging with limited ideas and scientific data to borrow from previous studies. The thesis is purely theoretical and consequently all the data generated and results obtained are ina simulated environment. The simulated data and results need technical judgment to rationalize.

6.2 Recommendation for Future Work

The system developed in this thesis assumes linear acoustic propagation. In practice, however, this may not always be the case. It would be beneficial to expand on the model such that it may capture nonlinear effects (such as attenuation with frequency dependence) although this greatly increases the complexity and considering the effect of reverberation in US imaging. Additionally, collecting the source signal practically from ultrasonic transducers could be of interest. Moreover, consideration of reverberant echoes and scientifically verified acoustic impedance of skin sub-layers could make the Cepstral analysis more realistic. This is due to the fact that there is no widely agreed upon published data that exists for all the acoustic properties of the skin layers and sub-layers.

References

[1] T. M. Robinson, “Basic principles of ultrasound.” Physics for Medical Imaging Applications, vol. 240, pp. 101–110, 2004.

[2] N. Waingankar, E. Goldenberg, and B. R. Gilbert, “History of ultrasound,” Ultrasound Male Genitalia, vol. 78, no. 2, pp. 1–9, 2015.

[3] A. F. Brown and J. P. Weight, “Generation and reception of wideband ultrasound,” vol.12, no. 4, pp. 161–167, 1974.

[4] R. H. Silverman et al., “The effect of transducer bandwidth on ultrasonic image characteristics,” vol. 15, no. 1, pp. 37–42, 1995.

[5] J. Viti, “High Framerate Imaging of Ultrasound Contrast Agents,” [Online]. Available: http://repub.eur.nl/pub/, accessed on August 2020.

[6] T. Penick, “Engineering Acoustics,” [online], availble: www.teicontrols.com/notes, pp. 1–36, 2002.

[7] S. Hughes, “Medical ultrasound imaging,” Phys. Educ., vol. 36, no. 6, pp. 468–475, 2001.

[8] W. Lee and Y. Roh, “Ultrasonic transducers for medical diagnostic imaging,” Biomed Eng Lett., vol. 7, no. 2, pp. 91–97, 2017.

[9] T. Wang, T. Kobayashi, and C. Lee, “Micromachined piezoelectric ultrasonic transducer with ultra-wide frequency bandwidth,” Appl. Phys. Lett., vol. 106, no. 1, pp. 1–6, 2015.

[10] L. West, “Cepstral Analysis of Wide-Band Ultrasound”, [Unpublished master thesis], University of Witwatersrand, South Africa, 2018.

[11] J. O. De Jesus, L. Parker, A. J. Frangos, and L. N. Nazarian, “Accuracy of MRI, MR arthrography, and ultrasound in the diagnosis of rotator cuff tears: a meta analysis", AJR Am J Roentgenol, vol. 192, no. 6, pp. 1701–1707, 2009.

[12] M. A. B. Postema, “Discrimination between quarry blasts and micro-earthquakes using spectral analysis , applied to local Israeli events,” Most, pp. 1–18, 1996.

[13] G. Baum, Fundamentals of medical ultrasonography, Putnam, 1975.

[14] A.M. Noll and M. R. Schroede, "Cepstrum pitch determination", The journal of the acoustical society of America, 41, pp. 293-309, 1967.

[15] P. Sharer, B. P. Goertz-allmann, “Spectral Studies of Shallow Earthquakes and Explosions : Implications for P/S Energy Partitioning, Stress Drop, and Discrimination,” Inst. Geophysics and Plantary Physics, January 2008.

[16] R. B. Randall, “Cepstrum Analysis and Gearbox Fault Diagnosis.,” Maint. Manag. Int., vol. 3, no. 3, pp. 183–208, 1982.

[17] C. Edwards, M.Aboosi, and R. Marks, "The use of A-scan ultrasound in the assessment of small skin tumours", Br J Dermaol., vol. 121, no. 3, pp. 297–304, 1989.

[18] C. Harland, J. C. Bamber, B. A. Gusterson, and P. S. Mortimer, "High frequency, high resolution B-scan ultrasound in the assessment of skin tumours," vol. 128, no. 5, pp. 525–532, 1993.

[19] A. V. Oppenheim, R. W. Schafer and J. R. Buck, "Discrete Time Signal Processing", Pearson, 3rd edition, 2010.

[20] K. Suzuki et al., "Ultrasonic tissue characterization of chronic liver disease using cepstral analysis," Gastroenterology, vol. 101, no. 5, pp. 1325–1331, 1991.

[21] T. A. Bigelow et al., "The Thermal Index," J. Ultrasound Med., vol. 30, no. 5, pp. 714–734, 2011.

[22] M. C. Ziskin, "Fundamental physics of ultrasound and its propagation in tissue.," Radiographics, vol. 13, no. 3, pp. 705–709, 1993.

[23] W. L Monsky, "The Evolution of Ultrasound Technologies; from Anatomic to Physiologic,Histologic, and Molecular Imaging," Anat. Physiol., vol. 04, no. 03, pp. 15–17, 2013.

[24] T. Szabo, "Diagnostic Ultrasound Imaging: Inside Out", Academic Press, chapter 3, pp. 55-80, 2013.

[25] J. T. Bushberg et al., The Essential Physics of Medical Imaging, 3rd edition, Lippincott Williams & Wilkins, 2013.

[26] P. Suetens, "Fundamentals of Medical Imaging", 2nd Ed., Cambridge University Press, pp 128-156, 2009.

[27] M. Feder and E. Weinstein, "Parameter Estimation of Superimposed Signals Using the EM Algorithm," IEEE Transaction on Acousics, Speech and Signa; Processing, vol. 36, no. 4, 1988.

[28] R. W. Cootney, "Ultrasound Imaging: Principles and Applications in Rodent Research," ILAR Journal, vol. 42, no. 3, 2001.

[29] W. M. Woo, "Skin Structure and Biology," Imaging Technol. Transdermal Deliv., pp. 1–14, 2019.

[30] J. Abdo, N. A. Sopko, and S. M. Milner, "The applied anatomy of human skin: A model for regeneration," Wound Med., vol. 28, no. September 2019.

[31] J. Kanitakis, "Anatomy, histology and immunohistochemistry of normal human skin," European journal of dermatology: EJD, vol. 12, no. 4, pp. 390–401, 2002.

[32] J. Sandby-Møller, T. Poulsen, and H. C. Wulf, "Epidermal Thickness at Different Body Sites: Relationship to Age, Gender, Pigmentation, Blood Content, Skin Type and Smoking Habits," Acta Dermato Venereologica., vol. 83, no. 6, pp. 410–413, 2003.

[33] A. Laurent et al., “Echographic measurement of skin thickness in adults by high frequency ultrasound to assess the appropriate microneedle length for intradermal delivery of vaccines,” Vaccine, vol. 25, no. 34, pp. 6423–6430, 2007.

[34] T. M. Robinson, “Basic Principles of Ultrasound imaging,” Springer, vol.240, NATO Science Series, pp. 101–110, 2007.

[35] D. Kireyev and J. Hung, Basics of Ultrasound Physics, Springer, Chapter 1, pp 1-8, 2016.

[36] I. Rudnick, “The Propagation of an Acoustic Wave along a Boundary,” Journal of the Acoustical Society of America., vol. 19, no. 2, pp. 348–356, 1947.

[37] J. Swanevelder, “Resolution in ultrasound imaging,” Continued. Education. , vol. 11, no. 5, pp. 186–192, 2011.

[38] T. A. Bigelow et al., “The Thermal Index Strengths, Weaknesses, and Proposed Improvements,” J. Ultrasound Med., vol. 30, no. 5, pp. 714–734, 2011.

[39] F. Hägglund, "Characterization of Thin Multi-Layered Materials Using Ultrasound", PhD Dissertation, Lulea University of Technology, Lulea, Sweden, 2009.

[40] W. Zhou, “Ultrasound Testing System for the Detecting of the Shape and Growth of a Vapor Chamber in the VAPEX Process,” University of Regina, July, 2011.

[41] P. Hoskins, “Physical principles of medical ultrasonics (2nd edition),” Ultrasound Medical Biology, vol. 30, no. 5, pp. 703, 2004

[42] C. M. Sehgal and J. F. Greenleaf, “Scattering of ultrasound by tissues,” Elseiver, vol. 6, no. 1, pp. 60–80, 1984.

[43] M. Bruneau, “Fundamentals of Acoustics,” ISTE Ltd. ISBN: 9781847045751, pp. 169-214, 2006.

[44] X. Fan, “The effect of wave reflection and refraction at soft tissue interfaces during ultrasound hyperthermia treatments,” Pubmed, vol. 91, March 1992, pp. 1727–1736, 1992.

[45] S. M. Bierig and A. Jones, “Accuracy and cost comparison of ultrasound versus alternative imaging modalities, including CT, MR, PET, and angiography,” Journal of Diagnostic Med., vol. 25, no. 3, pp. 138–144, 2009.

[46] D. C. Thielker and J. T. Jensen, "Introduction to Medical Physics", The American Journal of Nursing, vol. 62, no. 1. 1962.

[47] D. H. Johnston, M. N. Toksoz, and A. Timur, “Attenuation of Seismic Waves in Dry and Saturated Rocks.,” Geophysics, vol. 44, no. 4, pp. 691–711, 1979.

[48] K. K. Shung, “High Frequency Ultrasonic Imaging,” J Med Ultrasound, vol. 17, no. 1, pp. 25–30, 2009.

[49] J. Martinsson, J. E. Carlson, and J. Niemi, “Model-Based Phase Velocity and Attenuation Estimation in Wideband Ultrasonic Measurement Systems,” IEEE Trans

Ultrason Ferroelectr Freq Contorol, vol. 54, no. 1, pp. 138–146, 2007.

[50] J. C. Lacefield, "Physics of Ultrasound: a Handbook for Teachers and Students," IAEA, ISBN 978-92-0-131010-1, Chapter 12, 2013.

[51] P. E. S. Palmer, Manual of Diagnostic Ultrasound, Illustrated Ed., WHO, Chapter 3, 2003.

[52] L. Moraru, M. C. Nicolae, U. Dunarea, and L. Onose, "Ultrasound propagation through planar tissue layers," SISOM 2009 and Session of the Commission of Acoustics, Bucharest 28-29 May, 2002.

[53] N. Jiménez, J. Redondo, and F. Camarena, "Nonlinear ultrasound simulations including complex frequency dependent attenuation," Physics Procedia, vol. 63, no. December, pp. 108–113, 2015.

[54] E. Fermann et al. "Ultrafast Lasers: Technology and Applications," CRC Press, pp. 155–174, 2002.

[55] M. Tole, Harald Ostensen, "Basic physics of ultrasonic imaging", WHO, 2005.

[56] J. Swanevelder, "Resolution in ultrasound imaging," Continuing Education in Anaesthesia Critical Care & Pain, vol. 11, p. 5, 2011.

[57] J. Swanevelder, "Resolution in ultrasound imaging," Oxford University Press, vol. II, September 2011.

[58] E. Forman and R. Smith, "Documentation of peripheral nerve blockade : a complete audit cycle Survey of fatigue among trainee anaesthetists in the UK," Anaesthesia, vol. 72, pp. 11–106, 2017.

[59] T. L. Szabo, "Diagnostic Ultrasound Imaging: Inside Out ", Elsevier Academic Press, ISBN: 0-12-680145-2, 2004.

[60] D. Padfield, P. Mendonca, and S. Gupta, "Biomedical image analysis", CRC Press. pp. 61-90, 2015.

[61] X. Zeng, C. L. Yang, X. J. Zhou, and Y. C. Chen, "Ultrasonic Flaw Echoes Detection Based on Generalized S-Transform," Ultrasonic Methods, vol. 54, no. 2, pp. 137–145, 2018.

[62] R. B. Randall, "A history of cepstrum analysis and its application to mechanical problems,"Mech. Syst. Signal Process., vol. 97, pp. 3–19, 2017.

[63] B. P. Bogert, M. J. R. Healy, J. W. Tukey: "The Quefrency Alanysis of Time Series for Echoes: Cepstrum, Pseudo Autocovariance, Cross- Cepstrum and Saphe Cracking", Proceedings of the Symposium on Time Series Analysis (M. Rosenblatt, Ed) Chapter 15, 20, 1963.

[64] B. P. Bogert and J. F. Ossanna, "The Heuristics of Cepstrum Analysis of a Stationary Complex Echoed Gaussian Signal in Stationary Gaussian Noise," IEEE, vol. 12, no. 3, pp. 373-380, 1966.

[65] N. I. Nizam, S. R. Ara, K. Hasan, “Classification of Breast Lesions Using Quantitative Ultrasound Biomarkers,” Biomedical. Signal Process and Control, vol. 57, pp. 1–14, 2020.

[66] D. J. Cotter et al., “High Frequency Ultrasonic Thickness and Acoustic Velocity Measurement Methods for Advanced Material and Component Characterization,” 8th European Conf. on NDT, vol. 7, no. 10, pp. 1–11, 2020.

[67] K. A. Wear and S. Member, “Autocorrelation and Cepstral Methods for Measurement of Tibial Cortical Thickness,” IEEE, vol. 50, no. 6, pp. 655–660, 2003.

[68] D. C. Lay, S. R. Lay, and J. McDonald, "Linear algebra and its applications", Global Edition. 2017.

[69] M. Bruneau, Fundamentals of Acoustics, ISTE Ltd., ISBN: 9780470612439, pp. 30-54, 2006.

[70] S. F. Reis, “Characterisation of biological tissue: measurement of acoustic properties for ultrasound therapy,” 2013, [Online]. Available: http://repositorio.ul.pt//handle/10451/9598, Accesed on October 2020.

[71] S. Dykas et al., “Numerical method for modeling of acoustic waves propagation", Archives of Acoustics, vol. 35, no. 1, pp. 35-48, 2010.

[72] J. Martinsson, J. E. Carlson, and J. Niemi, “Model-based phase velocity and attenuation estimation in wideband ultrasonic measurement systems,” IEEE Trans on Ultrasonics, Ferroelctrics and Freq. Control, vol. 54, no. 1, pp. 138–146, 2007.

[73] S. I. Rokhlin and W. Huang, “Ultrasonic wave interaction with a thin anisotropic layer between two anisotropic solids, The Journal of the Acoustical Society of America, vol. 94, no. 6, pp. 3405–3420, 1993.

[74] F. Hägglund et al., “Model-based characterization of thin layers using pulse-echo ultrasound,” Proceedings of the International Congress on Ultrasonics, Vienna, April 9-13, 2007.

[75] F. Hägglund, J. Martinsson, and J. E. Carlson, “Flaw detection in layered media based on parametric modeling of overlapping ultrasonic echoes,” Proc. - IEEE Ultrason. Symp., vol. 1, pp. 136–139, 2006.

[76] R. Demirli and J. Saniie, “Model-based estimation of ultrasonic echoes part II: Nondestructive evaluation applications,” IEEE Trans on Ultrasonics, Ferroelctrics and Freq. Control, vol. 48, no. 3, pp. 803–811, 2001.

[77] R. Demirli and J. Saniie, “Model-based estimation of ultrasonic echoes part I: Analysis and algorithms,” IEEE Trans on Ultrasonics, Ferroelctrics and Freq. Control, vol. 48, no. 3, pp. 787–802, 2001.

[78] T. Merazi-Meksen, M. Boudraa, and B. Boudraa, “Ultrasonic Image Enhancement to Internal Defect Detection during Material Inspection,” MATEC Web Conf., vol. 208, pp. 0–3, 2018.